Architectural and facies organization of slope channel fills: Upper Cretaceous Rosario Formation, Baja California, Mexico

Pan Li [a, *], **Ben Kneller** [b], **Philip Thompson** [c], **Guilherme Bozetti** [b], Thisiane dos Santos [b]

[a] *Research Institute of Petroleum Exploration and Development, PetroChina, Beijing, 100083, China; formerly at* [b]

[b] *Department of Geology and Petroleum Geology, University of Aberdeen, AB24 3UE, UK*

[c] *Shell, UK*

Abstract

Slope channel systems, well-known for their significance in hydrocarbon exploration and sediment transport and deposition in deep-water settings, are inherently complicated in the rock record. To unravel the complexity, a better understanding of their internal organisation is needed. Here an integrated qualitative and quantitative examination of internal architecture and vertical facies successions is reported from the San Fernando slope channel system of the Rosario Formation (Maastrichtian), Baja California, Mexico. The San Fernando system (ca. 7 to 9 km wide, 400 m thick) comprises four channel complex sets (CCSs), of which this study focuses on the best exposed—CCS-B.

Geologic mapping and photomosaic interpretation indicate that CCS-B features an erosion-surface-bounded and coarse-grained lower succession that records braid-like channel fills at the channel belt axis. The overlying upper succession is characterised by fine-grained overbank or passive channel fills intercalated with conglomeratic sinuous channel fills at the channel belt axis. By contrast, fine-grained overbank deposits and a capping hemipelagic interval (abandonment) dominate the upper succession at the channel belt off-axis to margin.

Visual inspection of the measured sections from CCS-B suggests multiple fining-upward packages, which are partly confirmed by stochastic analysis of vertical facies transitions using the Markov chain technique. This technique also quantitatively demonstrates that distinct preferred vertical facies transitions characterise different stratigraphic levels (lower succession vs. upper succession), and varying depositional environments (axis vs. off-axis to margin) within the channel belt of CCS-B.

The results of this study merit close consideration as analogues to submarine channel systems characterised by a lower braided pattern and/or an upper meandering pattern, and should find wide applicability in subsurface prediction of reservoirs, in other outcrop-based studies, and in constraining transition probability-based stochastic geological modeling.

Keywords: Turbidite, Slope channel, Architecture organization, Vertical facies trend, Deep-water outcrop analogue

1. Introduction

Submarine channel systems, the major conduits for sediment transfer from continents to oceans, and significant hydrocarbon reservoirs in the subsurface, have been the focus of extensive research over more than forty years (e.g., Walker, 1975; Cronin, 1995; Campion et al., 2000; Cronin et al., 2000, 2005; Mayall and Stewart, 2000; Peakall et al., 2000; Sullivan et al., 2000; Camacho et al., 2002; Deptuck et al., 2003, 2007; Eschard et al., 2003; Fonnesu, 2003; Gardner et al., 2003; Kneller, 2003; Samuel et al., 2003; Beaubouef, 2004; Wild et al., 2005; Porter et al., 2006; Kane et al., 2007; Cross et al., 2009; Pyles et al., 2010; Di Celma et al., 2011; Hodgson et al., 2011; McHargue et al., 2011; Sylvester et al., 2011; Gamberi et al., 2013; Macauley and Hubbard, 2013; Hubbard et al., 2014; Li et al., 2016). These studies have improved our knowledge of submarine channel systems and, at the same time, highlighted the complexity and variability in their preserved stratigraphy. Despite this, there is only partially and qualitatively defined organisation of internal architecture and facies within submarine channel systems, and a better understanding of this would help not only in subsurface prediction of reservoirs, but also in enhancing stratigraphic and sedimentological models of deep-water systems. In these respects, exceptionally well-exposed large-scale outcrops are particularly useful, for they provide information on both large-scale architecture and small-scale facies, bridging the gaps in data resolution and scale of observation between seismic data and borehole data or limited small outcrops. Such studies have been reported widely, but mainly in a qualitative way, e.g., those documented from Canyon San Fernando, Mexico (Morris and Busby-Spera, 1990; Dykstra and Kneller, 2007), the Brushy Canyon, West Texas (Beaubouef et al., 1999; Gardner and Borer, 2000), the Pab Range, Pakistan (Eschard et al., 2003), the Magallanes basin, southern Chile (Crane and Lowe, 2008; Jobe et al., 2010), and the Karoo basin, South Africa (Hodgson et al., 2011; Figueiredo et al., 2013).

Here, an integrated qualitative analysis of internal architecture and quantitative analysis of vertical facies transitions is performed for the first time on an exhumed large-scale slope channel system. This slope channel system, ca. 7 to 9 km wide and 400 m thick, is located at Canyon San Fernando, Baja California, Mexico. It comprises four channel complex sets (*sensu* Campion et al., 2000; Sprague et al., 2002, 2005), of which this study focuses on the best-exposed, i.e. channel complex set B (CCS-B). In this study, architectural styles/elements from

different stratigraphic levels and spatial locations of CCS-B are documented qualitatively first, based on photomosaics, geological maps and cross sections, and measured sections. This is then followed by a statistical assessment of vertical facies trends, on the basis of Markov chain analysis of the vertical facies transitions documented in measured sections. The objective of this study is threefold: (1) to investigate the internal architecture of the slope channel fills, particularly at the scale of the channel complex set; (2) to examine the vertical facies trends of slope channel fills, and their implications for differentiating between internal architectural styles of a channel complex set; (3) to assess the applications of such an integrated qualitative and quantitative study to hydrocarbon exploration in channelized slope reservoirs.

2. Geological setting

2.1. Regional setting

The study area is located in the Rosario Embayment on the Pacific coast of Baja California, Mexico (Fig. 1a, b). The Rosario Embayment consists of Upper Cretaceous to Palaeocene sedimentary rocks that constitute part of the Peninsular-Ranges fore-arc basin complex (Morris and Busby-Spera, 1990). Sediments within the fore-arc basin were sourced from the Upper Jurassic to Upper Cretaceous former arc and associated batholiths to the east (Morris and Busby-Spera, 1990; Dykstra and Kneller, 2007). The depositional environments of these sediments alternated stratigraphically between continental and deep marine conditions (Fig. 1b, c), a trend that has been attributed to alternating uplift and down-dropping of the basin (Busby et al., 1998; Morris and Busby, 1996). These sediments in the Rosario Embayment are now disposed in a gently south-plunging syncline formed since the end of the Cretaceous, (Morris and Busby, 1996; Dykstra and Kneller, 2007) (Fig. 1b). The late Campanian to early Palaeocene Rosario Formation unconformably overlies the non-marine to shallow marine El Gallo Formation, and records a deepening-upward trend that consists of a lower fluvial-deltaic/shallow marine member and an upper deep-marine member (Morris and Busby-Spera, 1990). The upper, deep-marine member of the Rosario Formation comprises a submarine canyon-fill and an overlying channel-levee system (ca. 1 km thick), deposited over a period of about 1.6 Myr (Dykstra and Kneller, 2007), including the slope channel complex set investigated in this study. The Rosario Formation is capped unconformably by a kaolinitic palaeosol, which is in turn overlain by coastal to shallow marine sediments of the Palaeocene Sepultura Formation (Dykstra and Kneller, 2007; Kane et al., 2007) (Fig. 1c).

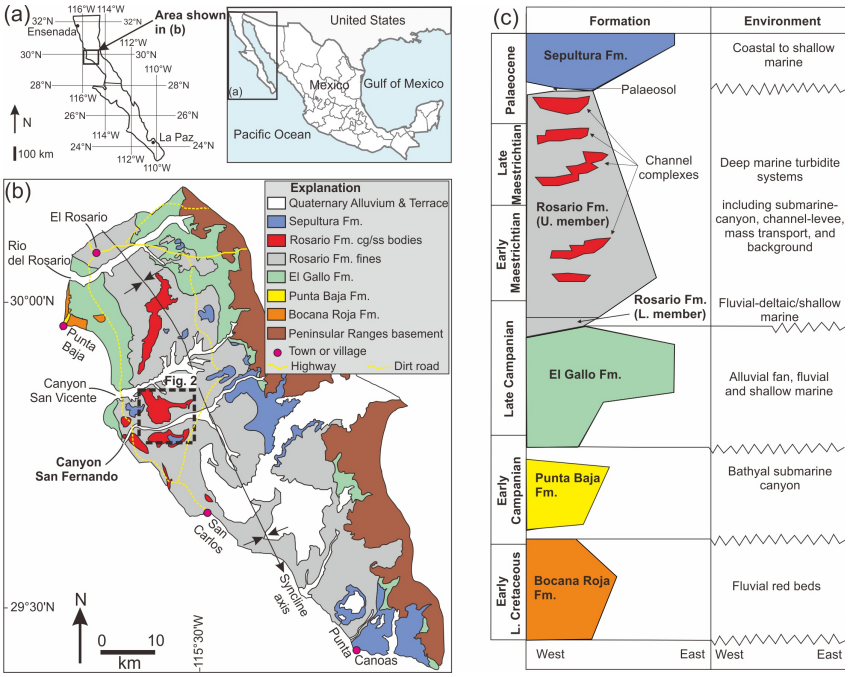

Fig. 1. (a) Location map showing the Rosario Embayment in Baja California, Mexico. (b) Regional geology of the Rosario Embayment of the Peninsular Ranges fore-arc basin complex (modified from Morris and Busby-Spera, 1990; Dykstra and Kneller, 2007). (c) Generalised stratigraphic column of the Rosario embayment (modified from Busby et al. 1998b; Dykstra and Kneller, 2007).

2.2. Canyon San Fernando

The study area lies in Canyon San Fernando, where a cross-sectional view of the slope channel system under discussion is exposed (Figs. 1, 2). It is located on the western limb of the regional syncline, with beds dipping gently (ca. 5 degrees) towards ENE. This superbly exposed slope channel system has been studied by various workers (Morris and Busby-Spera, 1990; Dykstra and Kneller, 2007; Kane et al., 2007, 2009; Thompson, 2010; Callow et al., 2013; McArthur et al., 2016) Hansen et al., 2017). In these studies, an overall bipartite large-scale architecture was reported, comprising a lower canyon fill and an upper channel-levee system. However, in this study, as in Hansen, et al. (2017), the lower canyon fill is considered to belong to a separate, older system (McArthur et al., 2016; the Playa Esqueleto system of Kane et al., 2009). The upper channel-levee system under discussion here is termed San Fernando slope channel system.

Comment [KPBC1]: Can't remove this bracket as it is inserted automatically Mendeley

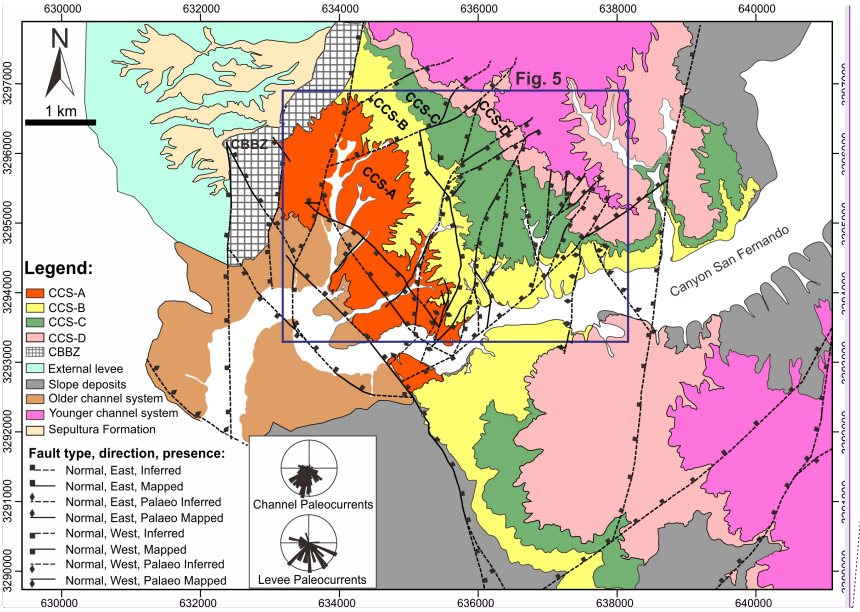

Fig. 2. Geological map of the Canyon San Fernando area, showing the four channel complex sets (CCS-A to CCS-D) within the channel belt, the channel belt boundary zone (CBBZ), the external levee to the NW, and slope deposits to the SE. The main palaeoflow is towards SSW, oblique to the regional WSW facing slope. Palaeoflow measurements are from Dykstra and Kneller, (2007). The boxed area indicates the region with detailed facies mapping (see Fig. 5). The numbers along the outer box indicate UTM coordinates.

The San Fernando slope channel system comprises a channel belt (ca. 5 to 7 km wide) that is confined to the NW by a well-developed external levee (ca. 2.5 km wide) and to the SE by an erosion surface cutting background slope hemipelagites. It thus shows a large-scale architectural asymmetry (Figs. 2, 3) (cf. Morris and Busby-Spera, 1990; Dykstra and Kneller, 2007; Kane et al., 2007). It can also be noticed that there is no discrete surface that separates the channel belt and the external levee. Instead, the “boundary” between them is characterised by a ca. 200 to 400 m wide transition zone with large (tens of metres across) slump blocks of the external levee (termed the channel belt boundary zone (CCBZ), sensu Hansen et al., 2017). Dominant palaeoflow of the channel belt of San Fernando slope channel system is towards SSW (220° to 230°, in contrast to a mean of 198° for the underlying older system mentioned above), implying the oblique orientation of channel belt to the WSW-facing regional slope, for which an underlying structural control is invoked (Dykstra and Kneller, 2007; Kane et al., 2007).

Within the channel belt, several erosional surfaces are present, traceable over several kilometers and with relief up to ca. 70m. These pronounced erosional surfaces and their

Comment [KPBC2]: You’ve described this ‘older channel system’ 9brown) as a canyon fill in the text. Must be consistent

corresponding conformable surfaces towards the marginal areas of the channel belt permit the subdivision of the channel system into four component channel complex sets, (sensu Sprague et al., 2002, 2005) referred to as CCS-A to CCS-D in ascending stratigraphic order (cf. Thompson, 2010; Hansen, 2016).

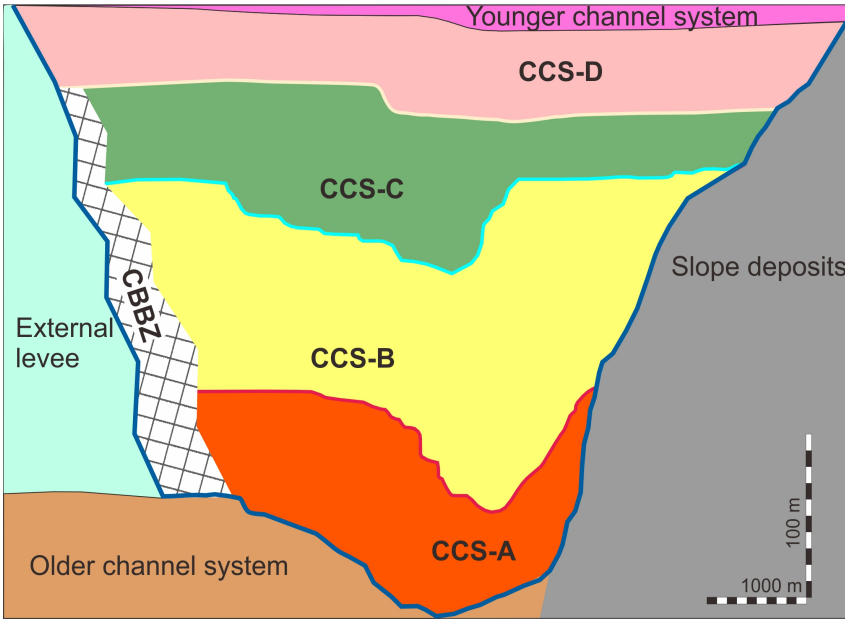

Fig. 3. Schematic cross section of the San Fernando slope channel system at the Canyon San Fernando area, showing the four channel complex sets (CCS-A to CCS-D) within the channel belt, the channel belt boundary zone (CBBZ), slope deposits and the external levee, as well as the overlying (Palaeocene) and underlying unrelated systems (modified from Thompson, 2010). See Fig. 2 for the corresponding geological map.

3. Data and Methodology

This outcrop-based study involves conventional mapping, digital mapping with a laser range-finder and hand-held computer (Trimble GeoXH 6000) with GNSS, high-resolution photomosaics, sketches, and sedimentary logs (totalling ca. 650 m) with palaeocurrent measurements. They are integrated so that geological maps, two-dimensional cross sections, and one-dimensional vertical successions are placed in context for analysis of the architectural and facies organization within CCS-B. A qualitative analysis of architectural patterns is conducted first, and then vertical facies trends are examined quantitatively by embedded Markov chain analysis.

3.1. Facies and architectural scheme

In this paper, we adopt a descriptive scheme of facies classficaiton based on dominant lithology and primary sedimentary characteristics (cf., Kane et al., 2009; Thompson, 2010), in contrast to the genetic schemes based on interpreted depositional processes or environments (e.g., Morris and Busby-Spera, 1990). A total of ten representative facies is recognised (summarised in table 1. and represented in Fig. 4). They could be grouped into five facies assemblages, with each containing >70% facies belonging to that particular assemblage. The facies assemblages are used as basic mapping units for architectural analysis (cf., Thompson, 2010), whilst the ten types of facies, coupled with significant erosional surfaces (relief >20 cm), serve as eleven different states in the statistical analysis of vertical trends using the embedded Markov chain technique.

This study focuses on CCS-A, one of the four genetically related architectural elements at the scale of channel complex sets that comprise the San Fernando channel system (channel complex system in the terminology of Sprague et al., 2002, 2005). Similarly to the other CCSs, CCS-A is marked by a regional major basal erosion surface (ca. 70 m relief), and at the top by a regional abandonment surface, or an erosion surface at the base of the succeeding CCS. CCS-A consists of at least four channel complexes, which are marked by basal erosion surfaces with relief up to 20-30 m and show distinct changes in architecture styles. Only the less amalgamated, uppermost channel complex within CCS-A could be unequivocally subdivided into channel elements (commonly ca. 10-15 m thick) that represent a single channel cycle from initiation to final abandonment (cf., Sprague et al., 2002). Channel elements could be further subdivided into bedsets, comprising one or several types of facies assemblages.

3.2. Embedded Markov chain analysis

Embedded Markov chain analysis is a statistical technique that can help objectively to assess whether the arrangement of different states (facies) in a certain succession is random or not (Gingerich, 1969; Krumbein and Dacey, 1969; Doveton, 1971; Carr, 1982; Powers and Easterling, 1982; Harper, 1984). This technique proves useful in establishing genetically related facies (facies associations *sensu stricto*), interpreting causal depositional processes and identifying distinct vertical facies trends associated with different architectural styles or elements (e.g., Miall, 1973; Martini et al., 1978; Haughton et al., 2003, 2009; Colombera et al., 2012; Sumner et al., 2012; Terlaky et al., 2016). Its application starts with testing the null hypothesis that a certain succession is made up of random/disordered states (facies). If this

null hypothesis can be rejected at a defined significance level by a chi-square test, it then follows that there is a certain degree of order within that succession (Lehrmann and Rankey, 1999). Following this, the technique then attempts to find those statistically significant transitions contributing to the order of the succession in question, by comparing observed transitions with expected transitions in random situations. The detailed step-by-step procedure can be found in Appendix A; see also Li, 2017 (see also Staňová et al., 2009). In this study, embedded Markov chain analysis has been applied to facies/facies assemblages plus erosional surfaces recorded in the measured sections of CCS-A. The final output for Markov chain analysis consists of a composite vertical section, observed facies frequency distribution, observed number of transitions between different facies (called observed transition count matrix), and a facies relationship diagram. The first three are used to visualize the original field data from different perspectives, and the last one is used to highlight preferred vertical facies transition trends.

Table. 1:
Facies assemblages and facies in the San Fernando slope channel system. See Fig. 4 for representative photographs of different facies.

Facies assemblage	Facies	Dominant lithology	Primary characteristics	Process interpretation
Mudstone facies assemblage (F1)	F1	Mudstone	Mainly massive with presence of carbonate concretions, trace fossils and microfossils (foraminifera) and common blueish colour, 5 cm to >10 m packages	Hemipelagic suspension fall-out and low-density turbidity currents
Heterolithic facies assemblage (F2)	F2	Thin-bedded mudstone and sandstone	Commonly normally graded and bioturbated, individual beds are usually less than 10 cm thick	Predominantly low-density turbidity currents
	F3-a	Structured sandstone	Parallel or ripple cross-laminated, fine to medium grained, usually normally graded, 10-30 cm thick	High- to low-density turbidity currents

Sandstone facies assemblage (F3)	F3-b	Structureless sandstone	Fine- to coarse-grained sand, graded or ungraded, 10 to 300 cm thick	High-density turbidity currents
	F3-c	Lithic pebbly sandstone	Structureless but commonly normally graded, lithic fragments mostly made of igneous rocks with rip-up mudstone clasts present locally, 5 to 150 cm thick	Predominantly high-density turbidity currents
Conglomerate facies assemblage (F4)	F4-a	Disorganised granules-pebbles	Clast-supported, granule- to pebble-grade conglomerate, structureless, ungraded without clast imbrication/organization, 10 to 200 cm thick	Debris flows (with subsequent winnowing) or bed-load transport beneath high-density turbidity currents
	F4-b	Organised granules-pebbles	Clast-supported, granule- to pebble-grade conglomerate, graded and/or showing clast imbrication/organization, 10 to 150 cm thick	Bed-load transport beneath high-density turbidity currents
	F4-c	Disorganised pebbles-cobbles	Clast-supported, pebble- to cobble-grade conglomerate, structureless, ungraded without clast imbrication/organization, 20 to 400 cm thick	Debris flows (with subsequent winnowing) or bed-load transport beneath high-density turbidity currents
	F4-d	Organised pebbles-cobbles	Clast-supported, pebble- to cobble-grade conglomerate, graded and/or showing clast imbrication/organization, 20 to 200 cm thick	Bed-load transport beneath high-density turbidity currents
Debrite facies assemblage (F5)	F5	Pebbly mudstone or muddy matrix - supported conglomerates	Matrix-supported, with varying percentage of intrabasinal or extrabasinal clasts, structureless, ungraded and disorganised, 10 to 700 cm thick	Debris flows
Erosional surfaces (Es)	Erosional surfaces with relief > 20 cm are treated as a special facies assemblage or facies for embedded Markov Chain analysis			

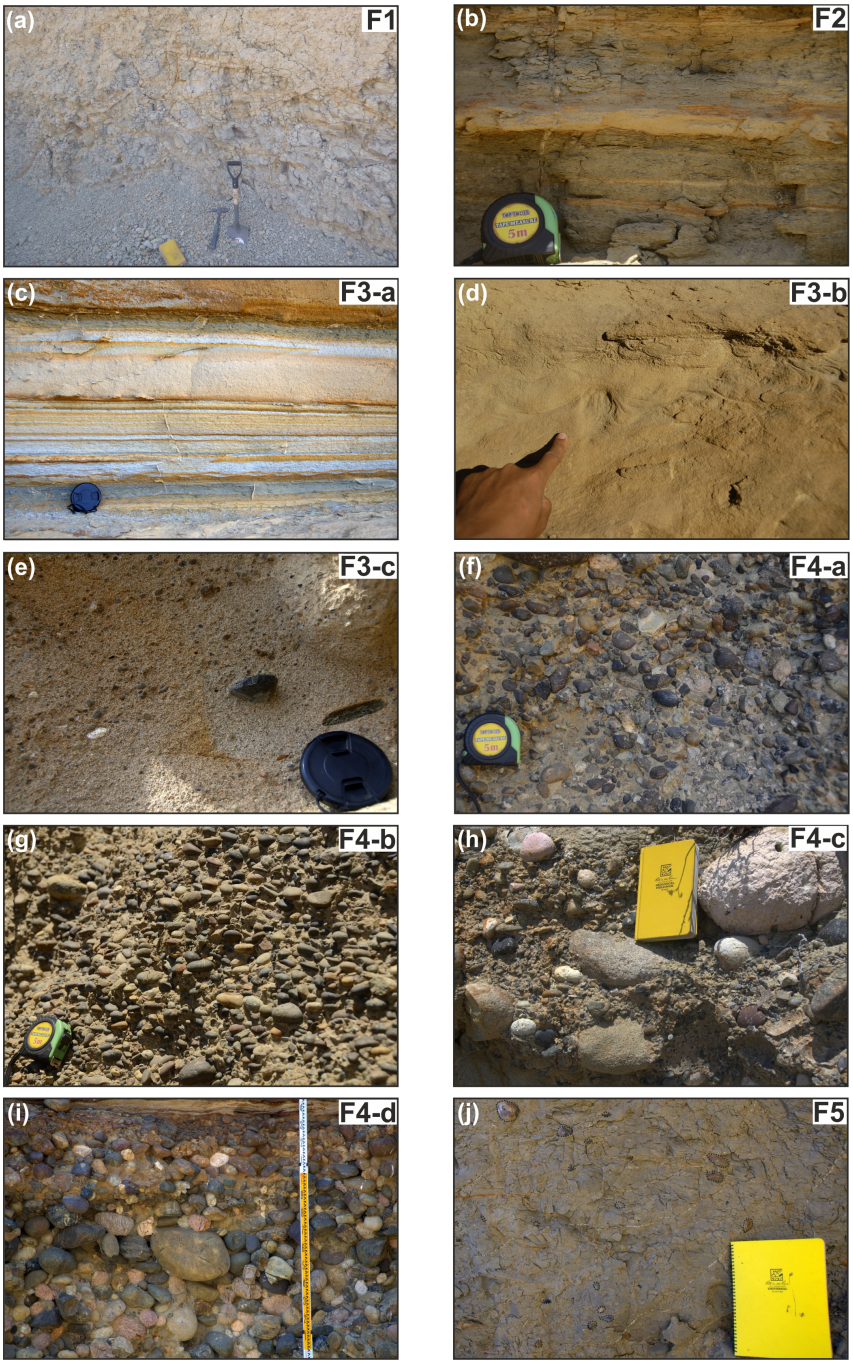
(a)
F1
(b)
F2
(c)
F3-a
(d)
F3-b
(e)
F3-c
(f)
F4-a
(g)
F4-b
(h)
F4-c
(i)
F4-d
(j)
F5

Fig. 4. Representative photographs of facies summarized in Table 1. (a) F1: mudstone. (b) F2: thin-bedded mudstone and sandstone. (c) F3-a: fine to medium grained, structured sandstone. (d) F3-b: fine- to coarse-grained structureless sandstone. (e) F3-c: lithic pebbly sandstone with scattered pebbles and rip-up mudstone clasts. (f) F4-a: disorganised granules to pebbles; (g) F4-b: organised granules-pebbles. (h) F4-c: disorganised pebbles-cobbles. (i) F4-d: organised pebbles-cobbles. (j) F5: Pebbly mudstone or matrix-supported conglomerates.

4. Architectural organization of channel complex set B (CCS-B)

Similarly to the other three channel complex sets within the San Fernando slope channel system, CCS-B features a lower succession (Stage I of Thompson, 2010) dominated by coarse-grained facies, which is bounded by a marked basal erosion surface; and a more heterogeneous upper succession (Stages II and III of Thompson, 2010) dominated by fine-grained facies stratigraphically punctuated by thin coarser-grained intervals (Figs. 5, 6). The architectural styles and component architectural elements associated with the lower and upper successions of CCS-B are discussed in detail below.

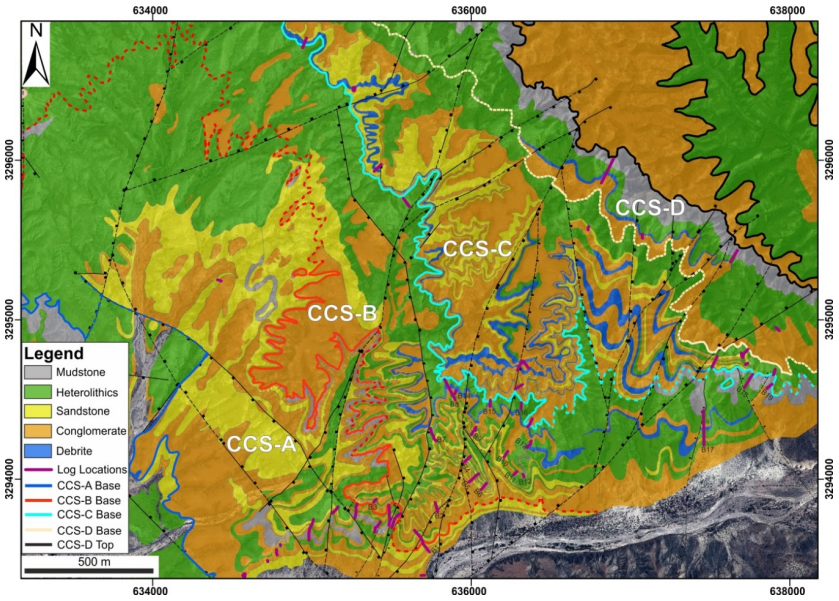

Fig. 5. Lithofacies map of the study area (see Fig. 2 for location), showing boundaries of channel complex sets, the distributions of different facies assemblages, and the locations of sedimentary logs within CCS-B.

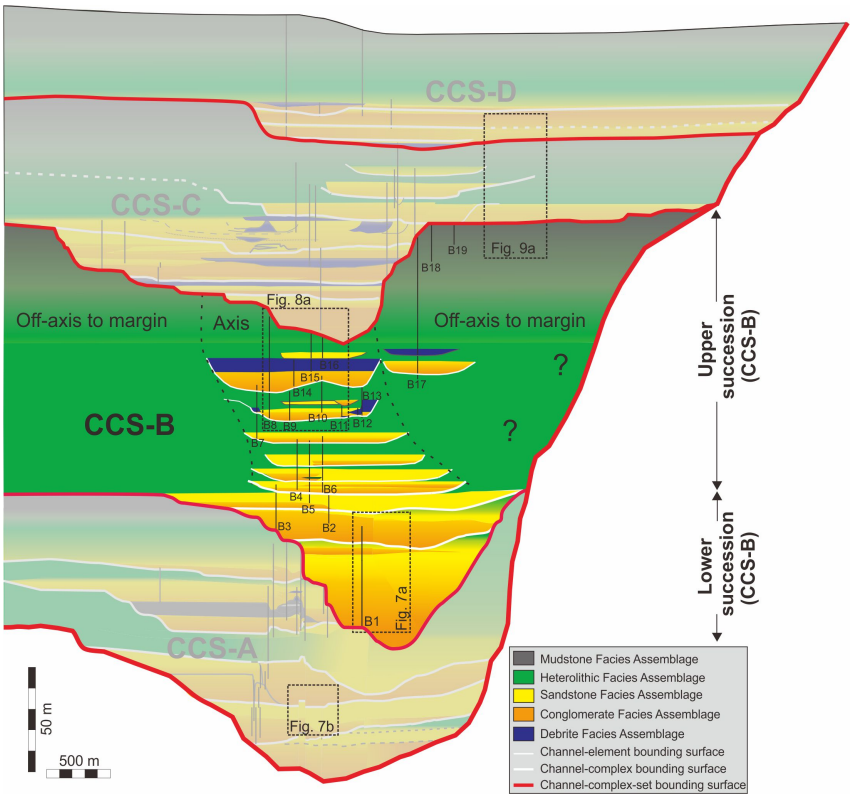

Fig. 6. Cross section of the channel belt within the San Fernando slope channel system (see Figs. 3, 5; palaeoflow out of the page), showing the multi-scale architecture elements and distributions of facies assemblages within the channel belt, with those belonging to CCS-B highlighted (focus of this study) and the rest shaded (modified from Thompson, 2010). B1-B19 indicates measured sections within CCS-B.

4.1. CCS-B lower succession

Description: A marked erosional surface underlying CCS-B lower succession is observed and mapped within the axial region of the channel belt (Figs. 5, 6). It incises into the underlying CCS-A to a maximum depth of approximately 70 m, and delimits highly-amalgamated conglomerates and sandstones (Facies assemblages F4 and F3) with subordinate debrites (F5) and very subordinate laterally discontinuous thin-bedded sandstones and mudstones (referred to hereafter as heterolithic sediments; F2) (Figs. 6, 7). Conglomerates (F4-c, F4-d) are predominantly large pebbles to cobbles in size with common rip-up mudstone clasts and transported blocks up to 2 m in the longest dimension. These conglomeratic deposits commonly form lenticular bodies with maximum thickness of 4 to 20 m, with clearly defined erosional bases

and scattered lenticular sandstone bodies (F3) (up to 0.1 to 2 m thick). Additionally, well-developed large-scale cross bedding, generally 1 to 2 m (up to 5 m) high, is commonly present in the conglomeratic lower successions of all the CCSs (Fig. 7). Conglomeratic packages tend to be capped by approximately tabular sandstone packages (mainly F3-b, F3-c) of a few metres thick, forming channel complexes with a broadly fining-upward profile (Fig. 7). Often these sandstones are excised by the erosion surface at the base of the overlying conglomeratic package, creating thick amalgamated composite bodies of conglomerate. Under these circumstances, it is challenging, if not impossible, to unequivocally define channel complexes, let alone to differentiate between smaller-scale channel elements and bedsets.

***Interpretation*:** CCS-B lower succession represents early-stage (Stage I of Thompson, 2010) confined channel fills at the channel belt axis. The pronounced basal erosion surface of CCS-B, its abundant internal erosion/amalgamation surfaces, coarse grain size, and a low proportion of fine-grained sediments suggest a high-energy, erosion- and bypass-dominated channel-belt axis environment. This environment corresponds to the deeply-entrenched and highly-confined part of the channel complex set and develops several distinct architectural elements: the prevailing erosive-based lenticular conglomerate and sandstone bodies represent cut-and-fill features within channel complexes. They record the punctuated incision and lateral migration of the active channel floors, and their subsequent filling. In contrast, the nearly flat-bottomed sheet-like sandstones suggest passive channel filling (i.e., channel backfilling processes during "relatively passive phases of channel activity", Wynn et al., 2007). Well-developed cross-stratified conglomerates indicate conglomeratic bars/bedforms, similar to those documented in the Cerro Toro Formation in southern Chile. Along with the abundant cut-and-fill structures and conglomerate-dominated nature with some clast imbrication, they bear strong similarities to some conglomeratic deep-water channel fills reported in other places where a braided channel belt is inferred (e.g., Winn and Dott, 1979; Hein and Walker, 1982; Hubbard et al., 2008; Di Celma et al., 2013). Taken together, we envisage that these coarse-grained sediments within the lower succession of CCS-B record fills of low sinuosity, braid-like channels within a confined submarine channel belt. A modern example of this style of channel systems is the Stromboli slope valley, south-eastern Tyrrhenian Sea (see Gamberi and Marani, 2011).

Comment [KPBC3]: Where is the reference?

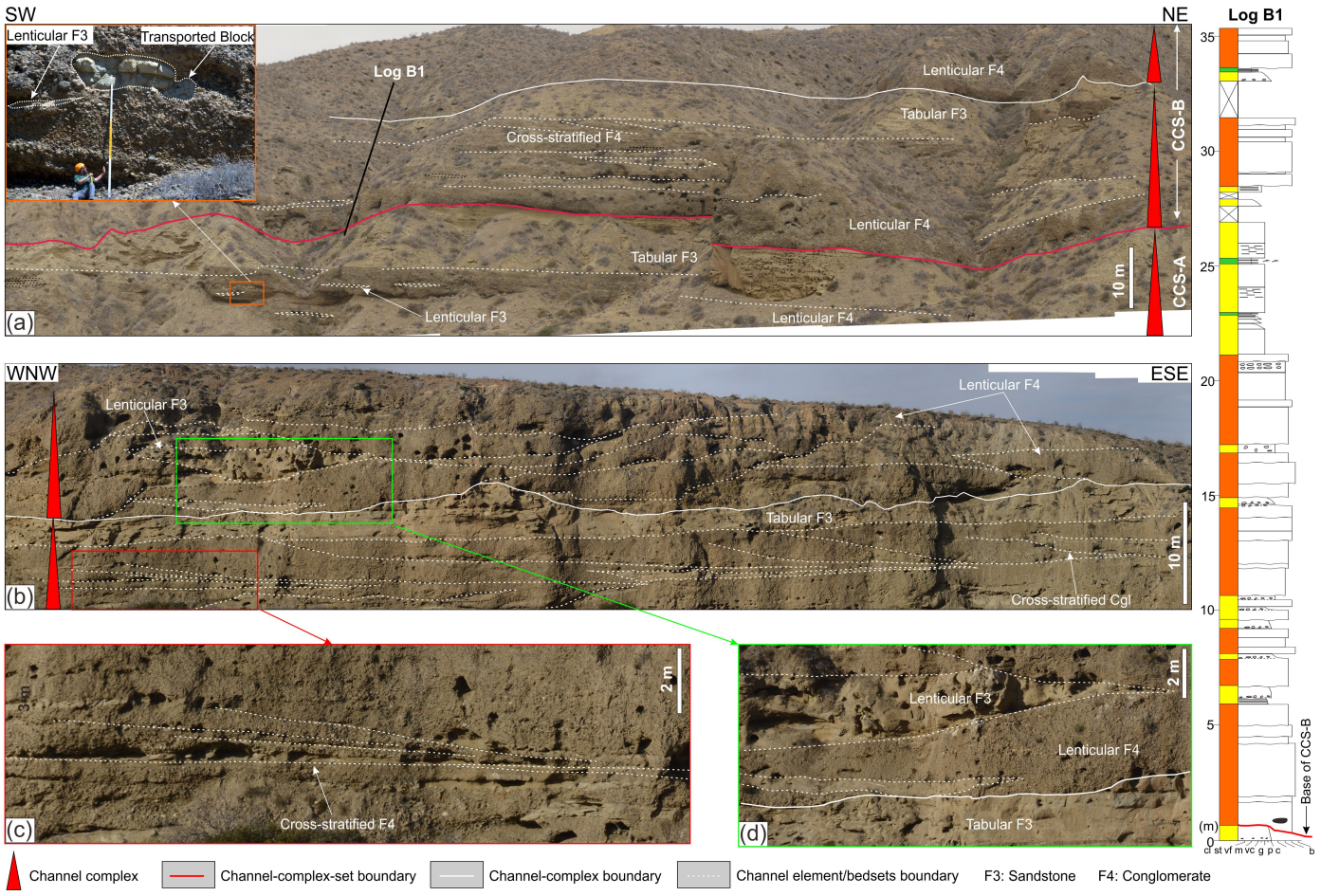
SW
NE
Log B1
Lenticular F3
Transported Block
Log B1
Lenticular F4
Tabular F3
Cross-stratified F4
Lenticular F4
Tabular F3
Lenticular F3
Lenticular F4
10 m
CCS-B
CCS-A
(a)
WNW
ESE
Lenticular F3
Lenticular F4
Tabular F3
10 m
Cross-stratified Cgl
(b)
3 m
2 m
Cross-stratified F4
(c)
2 m
Lenticular F3
Lenticular F4
Tabular F3
(d)
35
30
25
20
15
10
5
0
(m)
Base of CCS-B
d st vf f m vc g p c b
Channel complex
Channel-complex-set boundary
Channel-complex boundary
Channel element/bedsets boundary
F3: Sandstone
F4: Conglomerate

Fig. 7. Architectural features of the lower successions (Stage I) at the channel belt axis of channel complex sets A and B (CCS-A and CCS-B) (see Fig. 6 for location). (a) Photomosaic (approximately parallel to depositional dip (SSW)) and a measured section of the lower succession of CCS-B at the channel belt axis, where it incises into the upper part of CCS-A lower succession. Note the predominance of coarse-grained, amalgamated conglomerate (F4) and sandstone (F3), their geometries (lenticular or tabular), cross-stratification, and broadly fining-upward trends. (b) Photomosaic of CCS-A lower succession in a strike direction. Note the large-scale cross stratification (interpreted as bars/bedforms) (enlarged in c) and well-defined lenticular conglomeratic (F4) and sandy (F3) bodies (interpreted as scour fills) (enlarged in d).

4.2. CCS-B upper succession

In contrast to CCS-B lower succession, CCS-B upper succession (Stage II o) is dominated by thin-bedded heterolithic sediments (F2), with subordinate high aspect ratio (>20:1) conglomeratic and sandy bodies (F3, F4), mudstones (F1) and debrites (F5). The upper succession comprises two distinct regions, named herein the “axial area” and the “off-axis to marginal area”, which show contrasting architectural styles and components (see discussion below).

4.2.1 The axial area of CCS-B upper succession

Description: The axial area is a 2-3 km wide region where the intercalation of heterolithic sediments and laterally continuous but vertically isolated conglomeratic and sandy bodies dominates (Fig. 8). The conglomeratic bodies (ca. 5 m thick, 250 to 1500 m wide), generally made of finer-grained and better-organised conglomerates (F4-b, F4-d) than those in CCS-B lower succession, are tabular to slightly lenticular in shape. Internally, they show multiple sets of lateral accretion surfaces defined by thin intervening sand layers (F3-b, F3-c), with apparent dips of a few to fifteen degrees (Fig. 8). The sets of lateral accretion surfaces commonly show different dip directions and pass towards the channel cut banks into pebbly mudstone/muddy matrix-supported conglomerates (F5) (cf., Dykstra & Kneller, 2009; Janocko et al., 2013). Palaeocurrent measurements from some conglomeratic bodies show a relatively scattered pattern (Fig. 8). Stratigraphically, these conglomeratic bodies show minor incision into thin-bedded heterolithic sediments or sandstones, and are commonly capped by tabular sandstones (F3-a, F3-b) a few meters thick which, in turn, are overlain by thin-bedded heterolithic sediments. Alternatively, the conglomeratic bodies may be overlain directly by thin-bedded heterolithic sediments or pebbly mudstone. Laterally, these conglomeratic bodies pass into sandstones or thin-bedded heterolithic deposits (Fig. 8), although the exact lateral relationship (erosional vs. transitional) between them is not clear. In some places, lateral thinning and fining trends within the thin-bedded heterolithics-dominated sections could be observed, in which

mean palaeocurrent measurements (see Fig. 8) show a 30° to 60° difference from those in the overlying or underlying conglomeratic body.

***Interpretation*:** The axial area of CCS-B upper section represents later-stage fills (Stage II of Thompson, 2010) at the channel belt axis. These thin conglomeratic bodies with well-developed lateral accretion surfaces are comparable to the lateral accretion deposits within sinuous deep-water channels documented from the Ross Formation in Ireland, the Solitary channel in Spain, and elsewhere (e.g., Cronin, 1995; Haughton, 2000; Abreu et al., 2003; Arnott, 2007; Wynn et al., 2007; Janocko et al., 2013), in terms of their thickness, width and broadly fining-upward trends. These lines of evidence, coupled with their variable palaeocurrents, indicate that these thin conglomeratic bodies also represent lateral accretion deposits (LAPs of Abreu et al., 2003 and Dykstra & Kneller, 2009; LADs of Arnott, 2007) within channel elements, resulting from gradual lateral migration of sinuous channels without significant channel-floor aggradation (graded channels of Kneller, 2003). By contrast, the origins of the enclosing sandstones and thin-bedded heterolithic sediments are more uncertain owing to the limitations of exposure. They could represent the passive filling of these sinuous channels, during which the channel floor aggraded as a result of underfit through-going gravity flows (Wynn et al., 2007). Alternatively, they could be terraces, or internal levees *sensu* Kane & Hodgson, 2011, that formed due to overspilling of the upper, low-density portions of stratified turbidity currents passing through adjacent sinuous channels (cf., Piper et al., 1999; Dykstra & Kneller, 2009; McHargue et al., 2011; Hansen et al., 2015). The first mechanism is supported in places where sandstones onlap conglomeratic bodies or chaotic sediments that are confined by a clear erosional surface (e.g., Figure 11-45 of Thompson, 2010). However, an internal levee origin seems more likely for those thin-bedded heterolithic sediments that show lateral fining and thinning trends and overlie conglomeratic bodies with different mean palaeocurrent directions (Fig. 8).

Comment [KPBC4]: Add ref to Dykstra & Kneller 2009 – who Janocko ripped off!

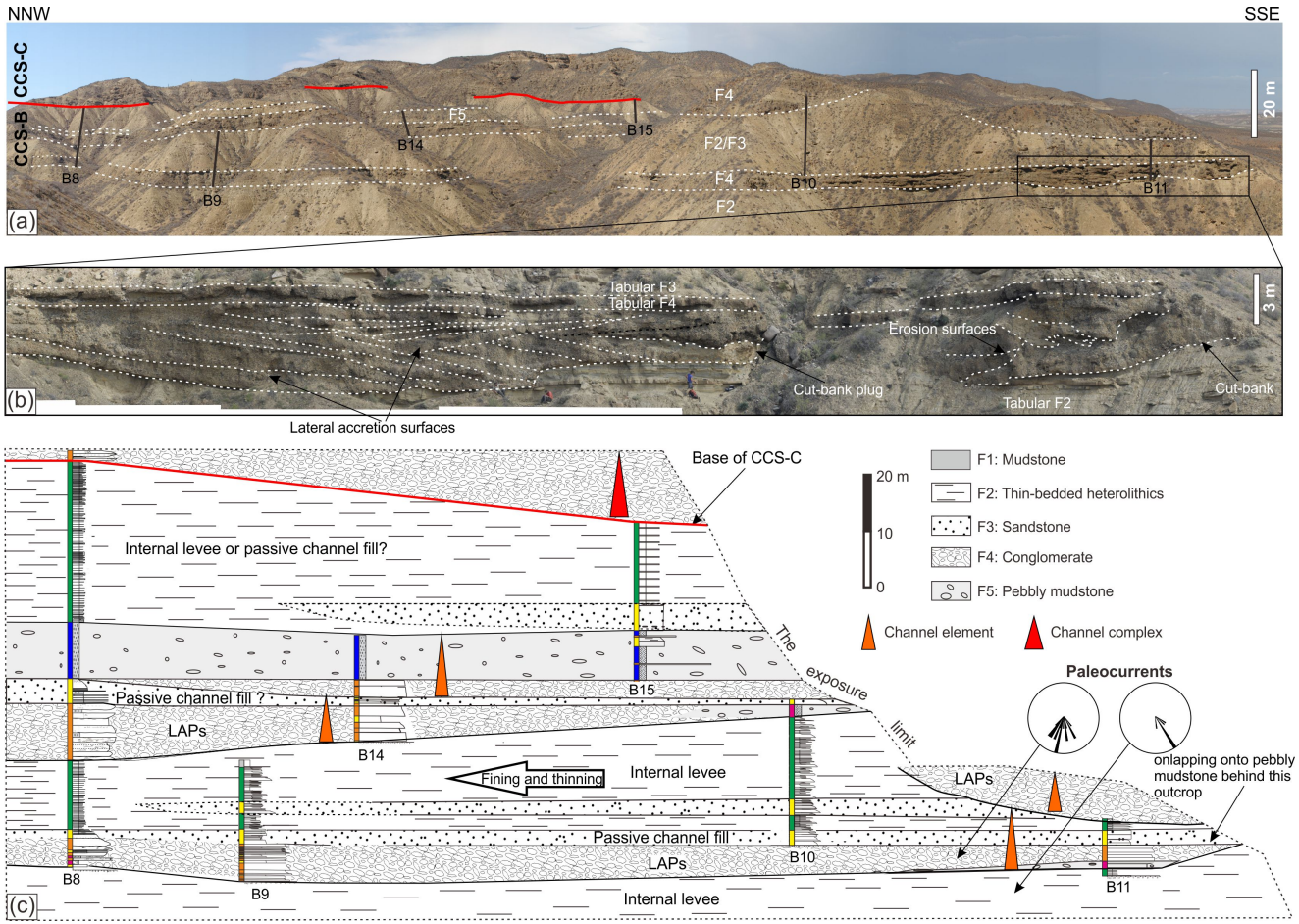
NNW
SSE
CCS-C
CCS-B
B8
B9
B14
F5
B15
F4
F2/F3
F4
F2
B10
B11
20 m
(a)
Tabular F3
Tabular F4
Erosion surfaces
Cut-bank plug
Tabular F2
Cut-bank
3 m
(b)
Lateral accretion surfaces
Base of CCS-C
Internal levee or passive channel fill?
Passive channel fill ?
LAPs
B14
B15
Fining and thinning
Internal levee
Passive channel fill
LAPs
B8
B9
B10
B11
Internal levee
The exposure limit
20 m
10
0
F1: Mudstone
F2: Thin-bedded heterolithics
F3: Sandstone
F4: Conglomerate
F5: Pebbly mudstone
Channel element
Channel complex
Paleocurrents
LAPs
onlapping onto pebbly mudstone behind this outcrop
(c)

Fig. 8. Architectural features of the axial area of CCS-B upper succession at the channel belt axis (see Fig. 6 for location). (a) Photomosaic of a region in the axial area of CCS-B upper succession with package boundaries and measured sections marked (see Fig. 6 for locations of these measured sections in the large-scale geological cross section). (b) Close-up view of the outlined area in (A), showing the architectural details of these conglomeratic lateral accretion packages (LAPs). Note the lateral accretion sets, cut-bank plug, and tabular conglomeratic and sandy bodies. (c) Detailed log correlation, showing the architectural styles and main component architectural elements in the axial area of CCS-B upper succession, including LAPs, passive channel fills, internal levees and pebbly mudstone channel plugs.

4.2.2 The off-axis to marginal area of CCS-B upper succession

***Description*:** The area of CCS-B upper succession lateral to the channel axis is dominated by discontinuously exposed thin-bedded turbidites (F2) (Hansen et al., 2017) and hemipelagic mudstones (F1) with carbonate concretions, microfossils, (e.g., foraminifera), and trace fossils (e.g., *Scolicia*, *Planolites* and *Ophiomorpha*) common in slope and basin floor settings in the Late Mesozoic to Early Cenozoic (e.g., Heard and Pickering, 2008; Cumming and Hodgson, 2011; Callow et al., 2013; Knaust et al., 2014). Hemipelagic mudstones are present as thin intervening layers in fine-grained and thin-bedded turbidite-dominated successions, or as the dominant component of a relatively thick capping package (up to 20 m thick) overlying the turbidite-dominated succession (Figs. 6, 9a). In addition to these fine-grained muddy sediments, subordinate thin (< 5m thick) and laterally continuous conglomeratic bodies (F4-b, F4-c, F4-d) with lateral accretion surfaces occur as discrete packages within them, as those well-exposed in the marginal areas of CCS-C upper succession (see Fig. 9b). They are comparable to those conglomeratic bodies in the axial area of CCS-B upper succession with respect to depositional character, but account for a smaller proportion of the succession and show a lower frequency of occurrence compared to the latter (Figs. 6, 9). Conglomeratic bodies are entirely absent in the most marginal areas. In addition, only infrequent and insignificant erosional surfaces (commonly with relief of less than 20 cm) are present in the off-axis to marginal area.

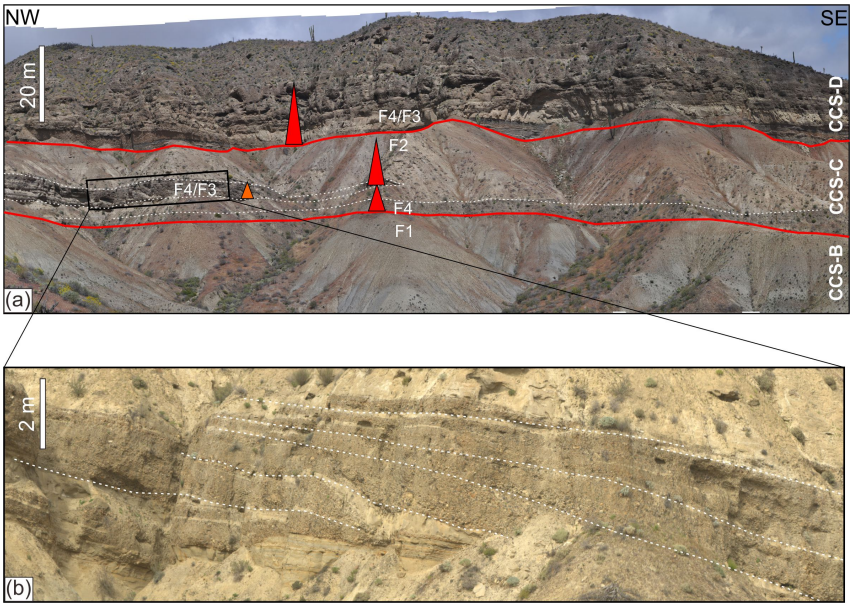

Fig. 9. (a) Architectural features of the marginal area of CCS-B, off-axis area of CCS-C and axial part of CCS-D (see Fig. 6 for location). Note the subordinate sandy (F3) or conglomeratic (F4) channel fills encased by thin-bedded heterolithic sediments (F2) of off-axis CCS-C, and dominant mudstone (F1) of the marginal area are of CCS-B. (b) Close-up of conglomeratic channel fills with well-developed lateral accretion surfaces; area highlighted in box in (a) (see text for discussion).

Interpretation: The lack of pronounced erosional surfaces, predominance of fine-grained turbidites and hemipelagic sediments with carbonate concretions and common deep-water micro- or trace fossils suggest a relatively low-energy and bathymetrically high region within the channel belt: the channel belt margin. Within this context, the fine-grained thin-bedded turbidite succession (Stage II of Thompson, 2010) is attributed primarily to overbank deposition (i.e., terraces/internal levees), resulting from the upper, low-density portions of turbidity currents, whose lower, high-density portions are confined predominantly within the channel belt axis and lesser extent to off-axis (cf., Morris and Busby-Spera, 1990; Kneller & Buckee 2000; Thompson, 2010; Hansen, 2016) (Fig. 6). By contrast, the overlying hemipelagite-dominated package (preserved only at the channel belt margin due to subsequent erosion at the base of CCS-C) represents a subsequent abandonment stage (Stage III of Thompson, 2010) with shut-down of gravity-flow sediment delivery in the channel system (cf., Nelson and Maldonado, 1988; Morris and Busby-Spera, 1990; Peakall et al., 2000; Kolla et al., 2012) (Fig. 6). The conglomeratic bodies embedded within the fine-grained turbidites of overbank origin are interpreted as lateral accretion deposits of sinuous channel elements in the off-axis region (in

proximity to the edge of the channel belt axis), based on their overall lower occurrence frequency than, and similar sedimentary characteristics to those observed in the channel belt axis (Fig. 9b).

5. Vertical facies trends of CCS-B

Embedded Markov chain analysis of the vertical facies transitions is applied to CCS-B on two different scales to test quantitatively the existence of vertical trends. On a large scale, the whole succession of CCS-B is evaluated, while on a smaller scale, the lower and upper successions are tested separately.

5.1. The whole succession of CCS-B

***Description*:** A composite stratigraphic succession made up of six measured sections (Fig. 10a) shows a large-scale broadly fining-upward trend in CCS-B, passing from a conglomerate-dominated succession through a thin-bedded turbidite-dominated succession to a locally preserved hemipelagic mudstone-dominated cap (Dykstra and Kneller, 2007; Thompson, 2010). Statistical analysis of the measured sections from CCS-B as a whole shows different occurrence frequencies for different facies assemblages and different vertical transitions between them (Appendix B of Li; see also 2016; Fig. 10b, c). In particular, the calculated chi-square test value of these vertical transitions substantially exceeds the limiting value, i.e. the threshold of rejecting a chi-square distribution at the significance level of 0.5% (Appendices A and B of Li, 2016; Fig. 10d). As a corollary, the probability of rejecting the null hypothesis of random facies transitions when it is true is thus less than 0.5% (cf., Doveton, 1971; Lehrmann and Rankey, 1999). Additionally, the facies relationship diagram shows two prominent, relatively simple up-stratigraphy transition tendencies - from erosional surface (Es) through conglomerate facies assemblage (F4), sandstone facies assemblage (F3), heterolithic facies assemblage (F2) to mudstone facies assemblage (F1); or from erosional surface (Es) to conglomerate facies assemblage (F4) to debrite facies assemblage (F5) (Appendices A and B; Fig. 10e).

***Interpretation*:** The large positive difference between the calculated chi-square test value and the limiting value indicates the presence of a very significant first-order Markov property (non-randomness) at the significance level of 0.5%. In other words, the succession of CCS-B as a whole shows an ordered vertical arrangement of facies assemblages at a confidence level of 99.5%. The order is expressed as fining-upward packages (tens of cm to ca. 20 m) indicated by the facies relationship diagram (Fig. 10e). This quantitatively demonstrates the existence of fining-upward trends that were tentatively defined in a qualitative manner in previous studies

Comment [KPBC5]: Exactly what constitutes 'very significant' in this context?

(e.g., Morris and Busby-Spera, 1990; Thompson, 2010). However, it should be noted that the largest scale fining-upward trend, i.e. the whole of CCS-B, can only be defined qualitatively here, due to insufficient data at this scale. The upward-decreasing depth of erosion surfaces, and consequent preservation of more overbank sediment higher in the succession may be responsible for this trend. It is also noteworthy that the debrite facies assemblage (F5) here appears at the end of a possible fining upward channel fill package in the upper succession of CCS-B, as those documented in the Geelbek channel from the Karoo basin (e.g., Brunt et al., 2013) (Fig. 8c, 10e). They are attributed to the temporary shut-down of late-stage channels within the CCS-B upper succession, where they have a relatively high preservation potential compared to earlier stages of channel development. This contrasts with many other case studies, where debrite facies assemblages are reported to be located mainly at the basal parts of channel systems and are thought of in these cases to be closely linked to initiation and bypassing of those systems. (e.g., Mayall and Stewart,2000; Samuel et al., 2003; Mayall et al., 2006).

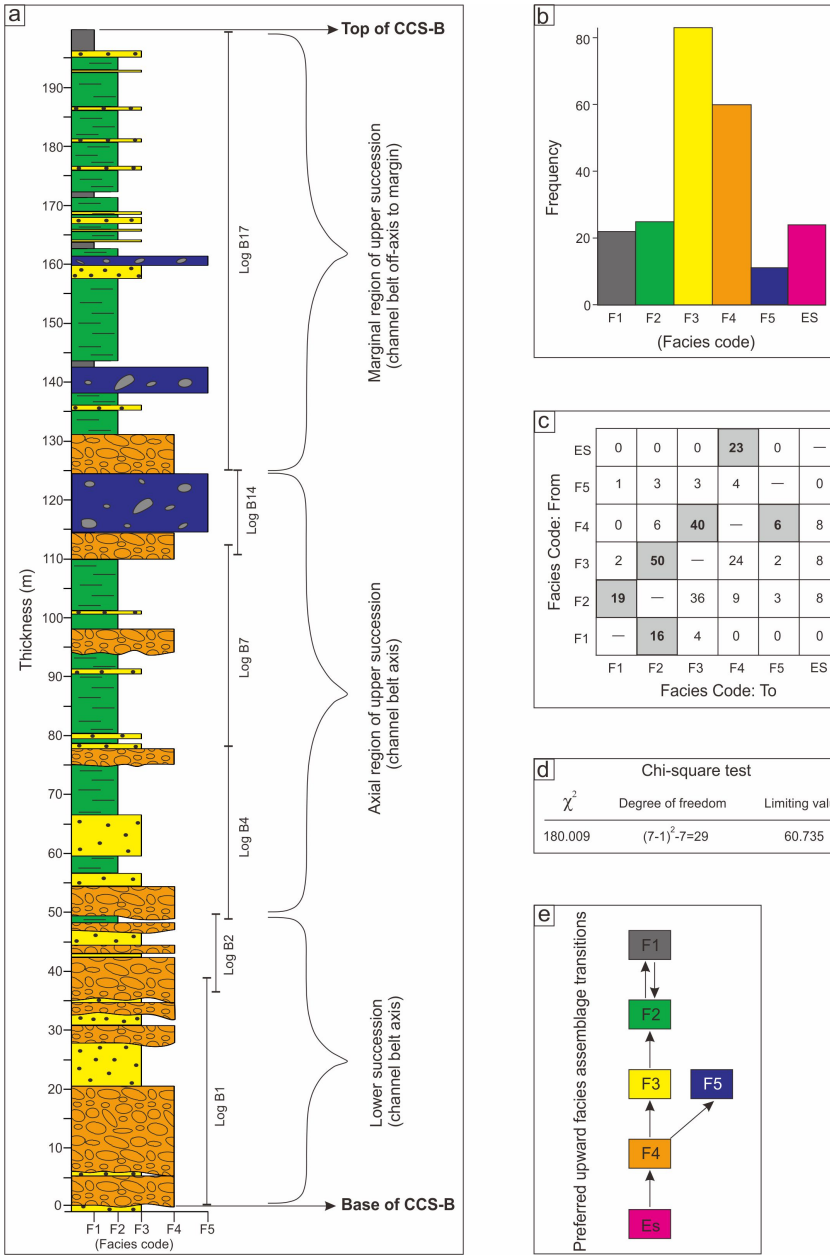

Fig. 10. The results of vertical facies transition analysis of the measured sections from CCS-B. (a) Composite stratigraphic succession based on six separate measured sections (log B1, B2, B4, B7, B14, B17 in Fig. 6). (b) Frequency distributions of different facies assemblages and erosional surfaces (with relief > 20 cm). (c) Observed transition count matrix with those significant transitions highlighted. (d) The chi-square test result, indicating the non-randomness (order) of vertical arrangement of facies. (e) Facies relationship diagram, showing the preferred

vertical facies assemblage transitions. Note the criterion of choosing “significant” transitions in (c) (and below in this study) is not the recorded number of transitions, but the difference between those recorded and those expected in a random situation (see Appendix A for more detailed explanation, and Appendix B of Li, 2016 for relevant parameters calculated in the Markov chain analysis). For explanation of facies codes, see Table 1.

5.2. CCS-B lower succession

***Description*:** The lower succession of CCS-B presents a wide range of sedimentary facies, but is dominated primarily by coarse-grained facies with common erosional surfaces (Fig. 11a-c). The calculated chi-square value is slightly larger than the limiting value at the significance level of 0.5% (Appendices A and C, Fig. 11d). Preferred vertical facies transitions of CCS-B lower succession are expressed as a long linear structure with two loops on the facies relationship diagram (Fig. 11e). The linear structure comprises an upward-coarsening segment represented by heterolithic turbidites (F2) → erosional surface (ES) → disorganised granule-pebble facies (F4-a) → organised granule-pebble facies (F4-b) → organised pebble-cobble facies (F4-d), which is followed by an upward-fining segment: disorganised pebble-cobble facies (F4-c) → pebbly sandstone (F3-c) → structureless sandstone (F3-b) → structured sandstone (F3-a).

***Interpretation*:** The insignificant difference between the calculated chi-square test value and the limiting value suggests a marginally significant first-order Markov property. The upward-coarsening and upward-fining trends revealed by the facies relationship diagram reflect waxing to waning flow energy cycles in the CCS-B lower succession (channel belt axis). Additionally, this ordered succession suggests a trend of deposition from earlier bed-load dominated, high-density turbidity currents, with or without debris flows, to later-stage low-density turbidity currents. This shows some resemblance to the well-known “Lowe sequence”, in which an upward transition trend from bed-load dominated, through high-density turbidity current suspension fall-out deposition to low-density turbidity current deposition is proposed (see Fig. 12 of Lowe, 1982). However, at the scale recorded here, the preferred vertical facies transitions represent the result of multiple flows rather than a single flow event (cf., Lowe, 1982).

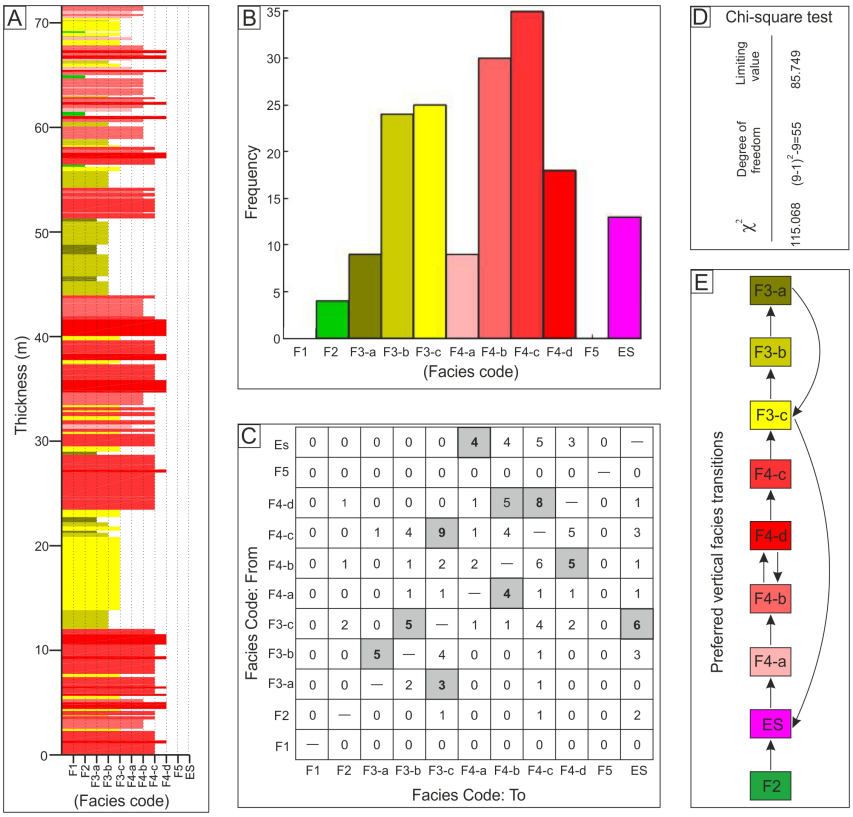

Fig. 11. The results of vertical facies transition analysis of the measured sections from CCS-B lower succession. (a) Composite stratigraphic succession based on three measured sections (B1, B2, and B3 in Fig. 6). (b) Frequency distributions of different facies and erosional surfaces (with relief > 20 cm). (c) Observed transition count matrix with those significant transitions highlighted. (d) The chi-square test result, indicating the non-randomness (order) of vertical arrangement of facies. (e) Facies relationship diagram, showing the preferred vertical facies transitions. See Appendix A and text for more detailed explanation of the embedded Markov chain analysis, Appendix C for relevant parameters calculated in the analysis, and Table 1 for explanation of facies codes.

5.3. CCS-B upper succession

5.3.1 The axial area of CCS-B upper succession

Description: The channel belt axis within CCS-B upper succession presents a very wide spectrum of sedimentary facies, with heterolithic turbidites as the dominant facies in terms of cumulative thickness and frequency (Fig. 12a-c). The chi-square test value of vertical facies transition counts is substantially larger than the limiting value at the significance level of 0.5% (Appendix A and D, Fig. 12d). In addition, the facies relationship diagram is characterised by two separate segments, which are made up of fine-grained facies associations and coarse-

grained facies associations respectively (Fig. 12e). The former is characterised by relatively simple vertical arrangements of four different types of facies, while the latter shows a very complicated vertical transition relationship between six different types of facies plus erosional surfaces with relief > 20 cm (Fig. 12e).

***Interpretation*:** The large positive difference between the calculated chi-square test value and the limiting value indicates the presence of a very significant first-order Markov property. This contrasts with the marginally significant Markov property within CCS-B lower section, suggesting the higher likelihood of non-randomness/order for vertical arrangement of different facies and erosional surfaces recorded in the axial area of CCS-B upper succession compared to CCS-B lower succession. The fine-grained and coarse-grained facies associations revealed by the facies relationship diagram (Fig. 12e) correspond respectively to heterolithic facies-dominated intervals (terraces/internal levees or passive channel fills), and conglomerate-dominated channel fills with lateral accretion deposits (LAPs) discussed in section 4.2 (Fig. 8). The latter are characterised by alternations of different facies suggesting common rhythmic variations in deposition pattern. This is attributed to the dynamic establishment of equilibrium channel geometry around the meander bends (Arnott, 2007). Notably, the dominant conglomeratic facies show well-developed fabrics (corresponding to facies F4-b and F4-d; see Figs. 4, 12b), suggesting significant bed-load traction deposition, which contrasts with the predominant suspension deposition suggested by Arnott (2007) for the conglomeratic lateral accretion deposits in the Isaac Formation, Canada. By contrast, the fine-grained facies associations are comparable to the so-called “classical turbidites” (partial or complete Ta to Te intervals of Bouma sequence; Bouma, 1962), and are attributed to waning low-density turbidity currents. The transition gap between the fine-grained and coarse-grained facies associations (see the two separate segments on the facies relationship diagram in Fig. 12e) indicates a non-systematic change from the conglomerate-dominated lateral accretion deposition to the thin-bedded heterolithic turbidites deposition. This might reflect the combined effects of multiple formative processes, such as channel migration/avulsion and channel abandonment.

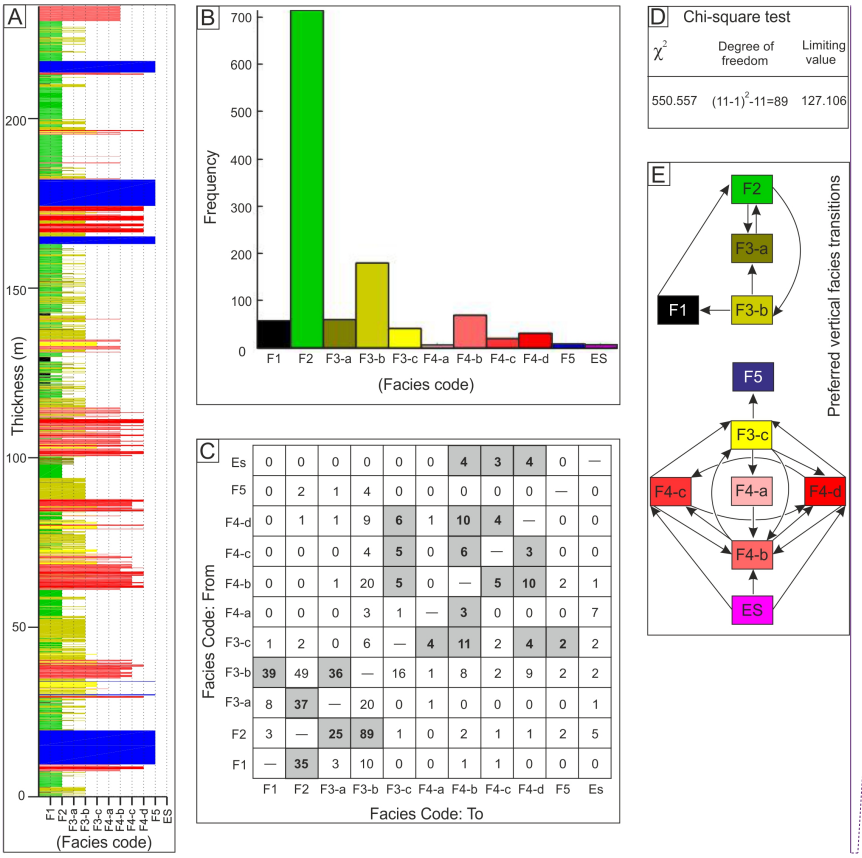

Fig. 12. The results of vertical facies transition analysis of the measured sections from the axial area of CCS-B upper succession. (a) Composite stratigraphic succession based on 13 measured sections (B4-B16 in Fig. 6). (b) Frequency distributions of different facies and erosional surfaces (with relief > 20 cm). (c) Observed transition count matrix with those significant transitions highlighted. (d) The chi-square test result, indicating the non-randomness (order) of vertical arrangement of facies. (e) Facies relationship diagram, showing the preferred vertical facies transitions. See Appendix A and text for more detailed explanation of the embedded Markov chain analysis, Appendix D for relevant parameters calculated in the analysis, and Table 1 for explanation of facies codes.

5.3.2 The off-axis to marginal area of CCS-B upper succession

Description: The off-axis to marginal area of CCS-B upper succession consists of thin-bedded heterolithic turbidites with many other subordinate facies types, and with a low frequency of coarser-grained conglomeratic facies (Fig. 13a-c). The calculated chi-square value of the transitions between different facies types also shows a substantially larger value (as above) than the limiting value at the significance level of 0.5% (Appendix E, Fig. 13d). Nevertheless, its vertical facies transition trends show a much simpler relationship, especially for the coarse-grained conglomeratic facies, in comparison to those in the channel belt axis

Comment [KPBC6]: The F5 colour on the transition diagram does not correspond to debrite colour on the log

within CCS-B upper succession (Figs. 12e, 13e). The fine-grained facies association shows a cycle that starts and ends with structureless sandstones (F3-b), whereas the coarse-grained facies association is characterised by alternations between organised granules-pebbles (F4-b) and disorganised or organised pebbles-cobbles (F4-c and F4-d, respectively) (Fig. 13e). Also noticeable is the weak tendency for structureless sandstone (F3-b) in the finer-grained facies association to be overlain by organised granules-pebbles (F4-b) in the coarser-grained facies association (Fig. 13e).

***Interpretation*:** A large chi-square test value compared to the limiting value at the defined significance level of 0.5% suggests a significant first-order Markov property, i.e. ordered vertical arrangement of facies in the off-axis to marginal area of CCS-B upper succession. Building on the architectural analysis discussed in section 4.2.2, the preferred vertical transition (F3-b → F3-a → F1 → F2 →F3-a) between the dominant fine-grained facies reflects the predominant deposition from waning low-density turbidity currents with intercalation of hemipelagic suspension at the channel belt margin. These low-density turbidity currents formed the thin-bed-dominated terraces/internal levees at the channel belt margin. The comparability between the above vertical facies trends and those for the fine-grained facies at the channel belt axis (see Fig. 12e) indicates that certain causal processes, such as channel overspilling and/or abandonment, are present across the channel belt. However, infrequent coarse-grained facies with simple vertical transitions and no marked erosional surfaces at the channel-belt off axis to margin suggest that competent gravity flows are likely to be uncommon in this region, and were highly variable. This, in turn, indicates significant bathymetric relief between the axial and marginal areas of the channel belt, which served to confine more competent and variable through-channel flows or their lower parts towards the bathymetric low (the axial area of the channel belt) (cf., Babonneau et al., 2002, 2010; Paull et al., 2011, 2013; Kolla et al., 2012; Gamberi et al., 2013). It may also indicate that there were periods when thin-bedded turbidites were accumulating in the axial region, when there was no significant gravel transport through the system.

Comment [KPBC7]: What is 'significant' in this context?

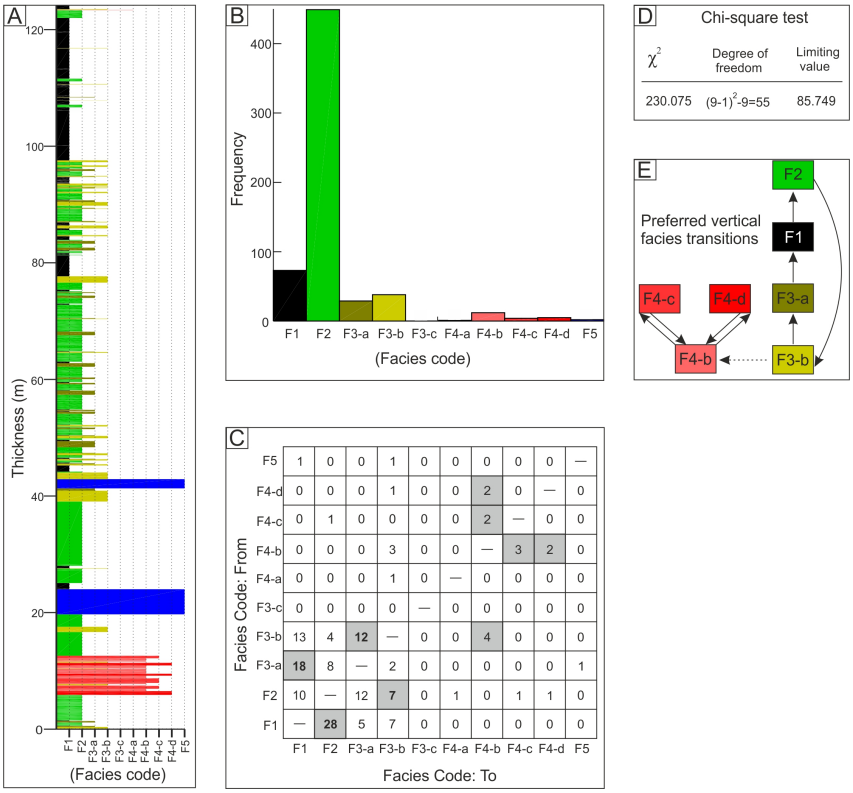

Fig. 13. (a) Composite stratigraphic succession of the off-axis to marginal area of CCS-B upper succession, showing the actual arrangement of different facies recorded from measured sections B17-B19 in Fig. 6. Note the predominance of mudstone or heterolithic facies. (b) Frequency distributions of different facies. Note the extremely high frequencies of fine-grained facies and the extremely low frequency of coarse-grained facies. (c) Observed transition count matrix with those significant transitions highlighted. (d) Chi-square test result, indicating the non-randomness (order) of vertical arrangement of facies. (e) Facies relationship diagram, showing the relatively simple vertical transition relationships between different facies types. See Appendix A and text for more detailed explanation of the embedded Markov chain analysis, See Appendix E for relevant parameters calculated in the analysis, and Table 1 for explanation of facies codes

6. Discussion

6.1. Expression of stratigraphic order within slope channel fills

Slope channel fills generally show neither completely deterministic nor random patterns. Rather, they lie somewhere between these two end-members, as with most other depositional systems on Earth (e.g., Hein et al., 1991; Wilkinson et al., 2004; Burgess, 2016). This is especially clear for slope channel fills at the scale of the channel system and its major building block (channel complex set), in which stratigraphic order is expressed in their architectural and

facies organization (e.g., Sprague et al., 2002, 2005; Deptuck et al., 2003; Porter et al., 2006; Di Celma et al., 2011, 2013; McHargue et al., 2011).

The stratigraphic succession at the channel system scale in the study area is characterised by various systematic vertical trends, including up-stratigraphy decreases in the basal erosional relief, average thickness and maximum grain sizes of its component channel complex sets (Figs. 3, 6). At the scale of the channel complex set, CCS-B shows clear vertical and lateral trends. Coarse-grained, highly amalgamated braid-like channel fills with bars/bedforms and abundant cut-and-fill structures dominate its lower succession at the channel belt axis, which is bound by its pronounced basal erosion surface (Figs. 6, 7). In contrast, thin-bedded fine-grained turbidites (terraces/internal levees or passive channel fills) with common intercalation of coarse-grained lateral accretion bodies (sinuous channel fills) dominate CCS-B upper succession at the channel belt axis (Figs. 6, 8). At the channel belt margin, thin-bedded fine-grained levee/terrace deposits predominate, with a hemipelagic mudstone interval (abandonment) at the top of CCS-B upper succession (Figs. 6, 9). The stratigraphic organization of upper CCS-B is similar in general scale and architecture to those documented in many other submarine channel systems (e.g., Peakall et al., 2000; Sprague et al., 2002, 2005; Deptuck et al., 2003; Porter et al., 2006; Hodgson et al., 2011; McHargue et al., 2011; Kolla et al., 2012; Macauley and Hubbard, 2013), and bears close comparison with the architectural schemes of Campion et al. (2000, 2005) and Sprague et al. (2002, 2005), although it is not a universal trend (cf., Gardner et al., 2003; Crane and Lowe, 2008).

In addition, the vertical arrangement of facies within CCS-B shows some organised patterns, including multiscale fining-upward trends and preferred vertical facies transitions that vary from the channel belt margin to the axis (Figs. 10-13). Intriguingly, at the channel belt axis, CCS-B upper succession (Stage II) presents a higher likelihood of preferred vertical facies transitions than CCS-B lower succession (Stage I) does. This mirrors the commonly reported increase in organization of channel stacking patterns towards the later stages of evolution of submarine channel systems (e.g., Hodgson et al., 2011; McHargue et al., 2011; Covault et al., 2016).

6.2. Controls on stratigraphic order of slope channel fills

Stratigraphic order and arrangement of architecture and facies, has been attributed to either allogenic or autogenic drivers, or a combination of both (e.g., Mutti, 1985; Kneller, 2003; Posamentier and Kolla, 2003; Bouma, 2004; Kneller et al., 2009; Romans et al., 2009; Hodgson et al., 2011; McHargue et al., 2011). Allogenic waxing-waning cycles of flow energy (due to

factors such as sea-level changes, or concomitant climate change) may have led to temporal changes from erosion/bypass dominated to deposition/aggradation dominated processes during the evolution of this submarine channel system, via steepening or shallowing of the equilibrium profile (e.g. Pirmez et al., 2000; Kneller, 2003; McHargue et al., 2011). Allogenic drivers are inferred to be primarily responsible for the stratigraphic order within the channel complex set to documented above, by analogy with other studies on organization of submarine channel fills (e.g., Di Celma et al., 2010, 2011, 2013; Hodgson et al., 2011). As an example, CCS-B's basal erosion surface (up to 70 m deep and 2-3 km wide), albeit perhaps composite in nature, likely records the lowering of the equilibrium profile during the waxing phase of the channel complex set energy cycle; the net effect of a combination of erosional and depositional flows, over a range of timescales, was erosional. In contrast, its lower succession (braid-like channels) and upper succession (vertically-stacked sinuous channels with terraces/internal levees; Fig. 6), reflect respectively an early and late rise of the equilibrium profile during the waning energy phase (cf., Kneller et al., 2003; Hodgson et al., 2011; McHargue et al., 2011; Kolla et al., 2012; Macauley and Hubbard, 2013), implying overall a progressive reduction in flow efficiency, punctuated by reversals that resulted in erosion.

Changes in equilibrium profile play significant roles in channel morphology and facies distribution. An equilibrium profile that steepens only slowly generates little accommodation, resulting in the abundant cut and fill of the CCS-B lower sequence, and lack of vertical organisation reflected in the Markov chain analysis. More rapid profile adjustment and accompanying increased accommodation space (Pirmez et al., 2000; Kneller, 2003) enhances deposition both within the channel axis and in the overbank area within the channel belt, as the entire systems aggrades. Creation of accommodation by steepening of the equilibrium profile increases the probability of vertical channel stacking patterns (Pirmez et al., 2000; Kneller, 2003) and possibly increased channel relief (Hodgson et al., 2011). A vertically ordered pattern of channel stacking tends to increase the likelihood of non-randomness/order of overall vertical facies arrangement. This is interpreted to be mainly responsible for the higher degree of vertical facies ordering within CCS-B upper succession compared to its lower succession (Figs. 11-13). In fact the CCS-B upper succession shows periods of stable profile (zero accommodation creation, no aggradation, and lateral accretion) followed by episodes of aggradation and overbank sedimentation, a progression described by Peakall et al. (2000).

Nonetheless, there are at least two other mechanisms that might be responsible for the observed trends. Firstly rise in the equilibrium profile could induce passive channel filling (cf.,

channel backfilling processes in Gardner and Borer, 2000; Pickering et al., 2001; Campion et al., 2005 and Wynn et al., 2007), and a resultant fining-upward succession (Fig. 8). On the other hand, autogenic processes may affect the facies organization locally. For example, gradual migration or avulsion of sinuous channels could result in the emplacement of fine-grained channel marginal or overbank deposits on top of coarser-grained channel axial deposits, resulting in a fining-upward vertical succession (Fig. 8), as proposed by some previous workers in the study area (Morris and Busby-Spera, 1990) and elsewhere (e.g., Hein and Walker, 1982; Graham and Bachman, 1983; Walker, 1985; Wuellner and James, 1989; Wonham et al., 2000; Wynn et al., 2007). However, common avulsions in braid-like channels tend to reduce rather than increase the degree of facies ordering, because of the abrupt random juxtaposition of very different facies in such low-confinement channels (Wuellner and James, 1989).

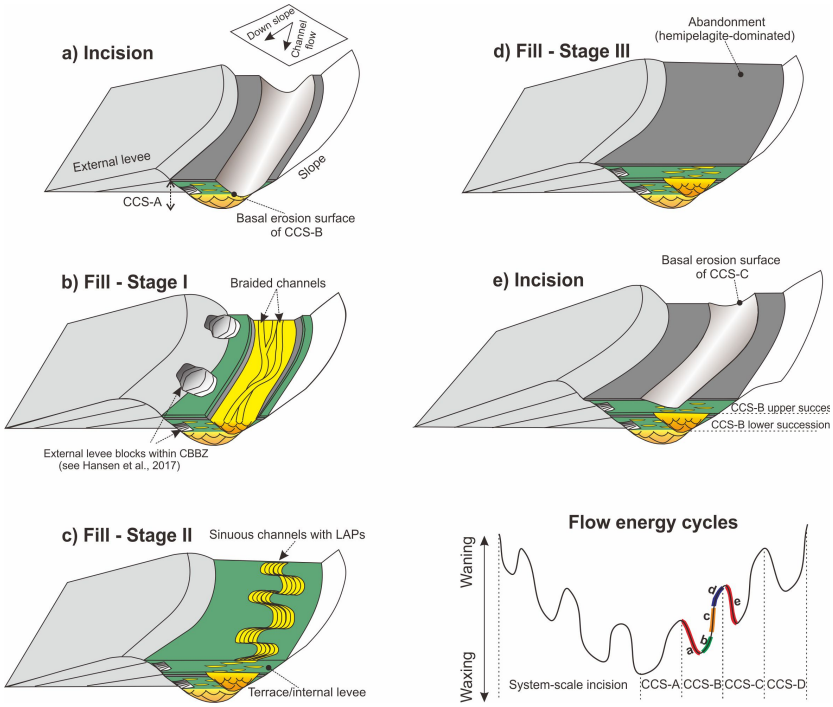

Fig. 14.

6.3. Implications for submarine channel reservoirs

CCS-B, as with many other channel complex sets in the study area and elsewhere (e.g., Sprague et al., 2002, 2005; Deptuck et al., 2003; Porter et al., 2006), reveals some predictable trends from a reservoir perspective. Highly-amalgamated, coarse-grained braid-like channel

fills deposited during the early stage of a channel belt development (e.g., those in the lower succession of CCS-B) tend to form reservoirs with good lateral and vertical connectivity. Individual channel bodies are likely to be poorly-defined and could develop an unresolvable composite architecture, especially on conventional industry seismic data (e.g., Samuel et al., 2003; Cross et al., 2009; Jackson et al., 2008). Laterally extensive coarse-grained meander belts formed of lateral accretion sets during the later stage of a channel complex set development (e.g., those in the CCS-B upper succession) show a ribbon-like geometry in plan form (cf., Peakall et al., 2000; Mayall et al., 2006; Wynn et al., 2007; Janocko et al., 2013). These will tend to form reservoirs with good lateral connectivity, but isolated from one another vertically by thin-bedded overbank/passive channel-filling turbidites, suggesting a low vertical connectivity.

This investigation into preferred vertical facies transitions in mixed coarse-grained and fine-grained slope channel fills demonstrates the potential of such an approach in analysis of submarine channel reservoir architecture based on 1-D vertical successions, such as hydrocarbon well data. Similar studies could be undertaken on other well-exposed submarine channel systems to build a large database in which the relationship between various architectural styles/elements and vertical facies transitions could be better constrained quantitatively. Such a large database, as the one built for fluvial channels by Colombera et al. (2012, 2013), could serve as a basis for comparison, interpretation and prediction for studies on submarine channel architecture in the subsurface.

7. Conclusions

The mixed coarse- and fine-grained channel complex set CCS-B represents a major building block of the slope channel system (ca. 7-9 km wide and 400 m thick) along Canyon San Fernando, Baja California, Mexico. Integrated qualitative and quantitative analysis shows that CCS-B shows a clearly defined stratigraphic organization in terms of cross-sectional architecture and vertical facies successions. It is bounded by an erosion surface ($a \leq 70$ m maximum relief) that is filled by a coarse-grained lower succession, representing braid-like channel fills at the channel belt axis. The overlying upper succession features LAP-dominated conglomeratic sinuous channel fills that are encased in thin-bedded, fine-grained sediments (overbank or passive channel fills) at the channel belt axis, and by thin-bedded, fine-grained terrace/internal levee deposits at the channel belt margin, capped by hemipelagic interval (abandonment) that is absent at the channel belt axis due to subsequent erosion beneath CCS-

C. The architectural organization of CCS-B is comparable to those associated with the erosional-to-aggradational trajectory of many submarine channel systems, and is attributed to the evolving equilibrium profile resulting from waxing-waning energy cycles driven by allogenic factors.

Vertical facies successions within CCS-B demonstrate some ordered arrangements. Firstly, multiscale fining–upward packages are recognized based on a combination of qualitative and quantitative approaches. Secondly, distinct preferred vertical facies transitions with differing likelihood, complexity in transition relationships and facies frequency distributions characterise different stratigraphic levels (lower succession vs. upper succession) and depositional settings (axis vs. off-axis to margin) within the channel belt of CCS-B (Figs. 11, 12, 13). The large-scale architectural organization and resulting non-random facies ordering is controlled largely by allogenic factors, though autogenic processes may also play a part (e.g., channel migration/avulsion).

The architectural similarities between this very coarse-grained system and those of finer grain-size (e.g. Morris et al., 2016) suggest that these features are largely grain-size independent. This suggests that the stratigraphic organization of CCS-B could serve as an analogue for comparable depositional systems, where channel complex sets consist of a lower braided pattern and an upper meandering pattern. The integrated approach utilised in this study could thus be applied elsewhere in order to develop quantitative generic architectural/facies models for such systems, and to differentiate their internal architecture.

Acknowledgments

This work comprised part of PL's PhD study, which was funded by the China Scholarship Council (CSC), and a research consortium including BG Group, BP, DONG, RWE Dea, Petrochina, Statoil and Tullow Oil. The authors thank all the many people associated with the deepwater research group at the University of Aberdeen, for their contributions to the mapping, description and interpretation of the study area, which provide the basis for this manuscript. Coding of the sedimentary logs and Markov chain analysis of coded logs were carried out respectively using the Matlab code (https://csdms.colorado.edu/wiki/Model:OptimalCycleID) of Peter Burgess, and by the program phpSediStat (http://phpsedistat.sourceforge.net/index.html) of Staňová Sidónia, Soták Ján and Hudec Norbert. We thank the reviewers …….. and ……. for their helpful and constructive comments.

References

Abreu, V., Sullivan, M., Pirmez, C., Mohrig, D., 2003. Lateral accretion packages (LAPs): an important reservoir element in deep water sinuous channels. Marine and Petroleum Geology 20, 631–648.

Arnott, R.W.C., 2007. Stratal architecture and origin of lateral accretion deposits (LADs) and conterminuous inner-bank levee deposits in a base-of-slope sinuous channel, lower Isaac Formation (Neoproterozoic), East-Central British Columbia, Canada. Marine and Petroleum Geology 24, 515–528.

Babonneau, N., Savoye, B., Cremer, M., Klein, B., 2002. Morphology and architecture of the present canyon and channel system of the Zaire deep-sea fan. Marine and Petroleum Geology 19, 445–467.

Babonneau, N., Savoye, B., Cremer, M., Bez, M., 2010. Sedimentary architecture in meanders of a submarine channel: detailed study of the present Congo turbidite channel (Zaiango project). Journal of Sedimentary Research 80, 852–866.

Beaubouef, R.T., Rossen, C., Zelt, F.B., Sullivan, M.D., Mohrig, D.C., Jennette, D.C., 1999. Deep-water sandstones, Brushy Canyon Formation, West Texas. American Association of Petroleum Geologists, Continuing Education Course Notes 40, 1–50.

Beaubouef, R.T., 2004. Deep-water leveed-channel complexes of the Cerro Toro Formation, Upper Cretaceous, southern Chile. AAPG Bulletin 88, 1471–1500.

Bouma, A.H., 1962. Sedimentology of Some Flysch Deposits: A Graphic Approach to Facies Interpretation. Elsevier, Amsterdam, 168 pp.

Bouma, A.H., 2004. Key controls on the characteristics of turbidite systems. In: Lomas, S.A., Joseph, P. (Eds.), Confined Turbidite Systems: Geological Society of London Special Publication 222, pp. 9–22.

Burgess, P., 2016. Identifying ordered strata: evidence, methods, and meaning. Journal of Sedimentary Research 86, 148–167.

Busby, C.J., Smith, D., Morris, W.R., Fackler-Adams, B.N., 1998. Evolutionary model for convergent margins facing large ocean basins: Mesozoic Baja California, Mexico. Geology 26, 227–230.

Callow, R.H.T., McIlroy, D., Kneller, B., Dykstra, M., 2013. Integrated ichnological and sedimentological analysis of a Late Cretaceous channel-turbidite system: the Rosario

Formation, Baja California, Mexico. Marine and Petroleum Geology 41, 277 – 294.

Camacho, H., Busby, C.J., Kneller, B., 2002. A new depositional model for the classical turbidite locality at San Clemente State Beach, California. AAPG Bulletin 86, 1543 – 1560.

Campion, K.M., Sprague, A.R., Mohrig, D., Lovell, R.W., Drzewiecki, P.A., Sullivan, M.D., Ardill, J.A., Jensen, G.N., Sickafoose, D.K., 2000. Outcrop expression of confined channel complexes. In:Weimer, P., Slatt, R.M., Coleman, J., Rosen, N.C., Nelson, H., Bouma, A.H., Styzen, M.J., Lawrence, D.T. (Eds.), Deep-Water Reservoirs of The World. Gulf Coast Section SEPM 20th Bob F. Perkins Research Conference, pp. 127 – 150.

Campion, K.M., Sprague, A.R., Sullivan, M.D., 2005. Architecture and lithofacies of the Capistrano Formation (Miocene-Pliocene), San Clemente, California. AAPG Fieldtrip Guidebook 100, SEPM, Fullerton Pacific Section, Fullerton, California, pp. 1 – 42.

Carr, T.R., 1982. Long-linear models, Markov chains and cyclic sedimentation. Journal of Sedimentary Petrology 52, 905 – 912.

Colombera, L., Felletti, F., Mountney, N.P., McCaffrey, W.D., 2012. A database approach for constraining stochastic simulations of the sedimentary heterogeneity of fluvial reservoirs. AAPG Bulletin 96, 2143 – 2166.

Colombera, L., Mountney, N.P., McCaffrey, W.D., 2013. A quantitative approach to fluvial facies models: methods and example results. Sedimentology 60, 1526 – 1558.

Covault, J.A., Sylvester, Z., Hubbard, S.M., Jobe, Z.R., Sech, R.P., 2016. The stratigraphic record of submarine-channel evolution. The Sedimentary Record 14, 4 – 11.

Crane, W.H., Lowe, D.R., 2008. Architecture and evolution of the Paine channel complex, Cerro Toro formation (Upper Cretaceous), Silla Syncline, Magallanes basin, Chile. Sedimentology 55, 979 – 1009.

Cronin, B.T., 1995. Structurally-controlled deep-sea channel courses: examples from the Miocene of South-east Spain and the Alboran Sea, South-west Mediterranean. In: Hartley, A.J., Prosser, D.J. (Eds.). Characterisation of Deep Marine Clastic Systems, vol. 94. Geological Society of London Special Publication, pp. 113 – 133.

Cronin, B.T., Hurst, A., Celik, H., Turkmen, I., 2000. Superb exposure of a channel, levee and overbank complex in an ancient deep-water slope environment. Sedimentary Geology 132, 205 – 216.

Cronin, B.T., Celik, H., Hurst, A., Turkmen, I., 2005. Mud prone entrenched deep-water slope channel complexes from the Eocene of eastern Turkey. In: Hodgson, D.M., Flint, S.. (Eds.),

Submarine Slope Systems: Processes and Products. Geological Society of London, Special Publications 244, pp. 155 – 180.

Cross, N.E., Cunningham, A., Cook, R.J., Taha, A., Esmaie, E., El Swidan, N., 2009. Three-dimensional seismic geomorphology of a deep-water slope-channel system: The Sequoia field, offshore west Nile Delta, Egypt. AAPG Bulletin 93, 1063 – 1086.

Cummings, J.P., Hodgson, D.M., 2011. Assessing controls on the distribution of ichnotaxa in submarine fan environments, the Basque Basin, Northern Spain, Sedimentary Geology 239, 162-187. doi: 10.1016/j.sedgeo.2011.06.009.

Deptuck, M.E., Steffens, G.S., Barton, M., Pirmez, C., 2003. Architecture and evolution of upper fan channel-belts on the Niger Delta slope and in the Arabian Sea. Marine and Petroleum Geology 20, 649 – 676.

Deptuck, M.E., Sylvester, Z., Pirmez, C., O'Byrne, C., 2007. Migration–aggradation history and 3-D seismic geomorphology of submarine channels in the Pleistocene Benin-major Canyon, western Niger Delta slope. Marine and Petroleum Geology 24, 406 – 433.

Di Celma, C., Cantalamessa, G., Didaskalou, P., Lori, P., 2010. Sedimentology, architecture, and sequence stratigraphy of coarse-grained, submarine canyon fills from the Pleistocene (Gelasian-Calabrian) of the Peri-Adriatic basin, central Italy. Marine and Petroleum Geology 27, 1340 – 1365.

Di Celma, C.N., Brunt, R.L., Hodgson, D.M., Flint, S.S., Kavanagh, J.P., 2011. Spatial and Temporal Evolution of a Permian Submarine Slope Channel–Levee System, Karoo Basin, South Africa. Journal of Sedimentary Research 81, 579 – 599.

Di Celma, C., Cantalamessa, G., Didaskalou, P., 2013. Stratigraphic organization and predictability of mixed coarse-grained and fine-grained successions in an upper slope Pleistocene turbidite system of the Peri-Adriatic basin. Sedimentology 60, 763 – 799.

Doveton, J.H., 1971. An Application of Markov Chain Analysis to the Ayrshire Coal Measures Succession. Scottish Journal of Geology 7, 11 – 27.

Dykstra, M., Kneller, B., 2007, Canyon San Fernando, Mexico: a deep-water, channel-levee complex exhibiting evolution from submarine canyon-confined to unconfined. In: Nilsen, T.H., Shew, R.D., Steffens, G.S., Studlick, J.R.J. (Eds.), Atlas of Deep-water Outcrops. AAPG Studies in Geology 56, pp. 226 – 230.

Dykstra, M., Kneller, B., 2009. Lateral accretion in a deep-marine channel complex: implications for channellized flow processes in turbidity currents. Sedimentology 56, 1411 – 1432.

Eschard, R., Albouy, E., Deschamps, R., Euzen, T., Ayub, A., 2003. Downstream evolution of turbiditic channel complexes in the Pab Range outcrops (Maastrichtian, Pakistan). Marine and Petroleum Geology 20, 691–710.

Figueiredo, J.P., Hodgson, D.M., Flint, S.S., Kavanagh, J.P., 2013. Architecture of a channel complex formed and filled during long term degradation and entrenchment on the upper submarine slope, Unit F, Fort Brown Fm., SW Karoo Basin, South Africa. Marine and Petroleum Geology 41, 104–116.

Fonnesu, F., 2003. 3D seismic images of a low-sinuosity slope channel and related depositional lobe (West Africa deep-offshore). Marine and Petroleum Geology 20, 615–629.

Gamberi, F., Marani, M., 2011. Geomorphology and sedimentary processes of a modern confined braided submarine channel belt (Stromboli Slope Valley, Southeastern Tyrrhenian Sea). Journal of Sedimentary Research 81, 686–701.

Gamberi, F., Dykstra, M., Kane, I.A., Kneller, B.C., 2013. Integrating modern seafloor and outcrop data in the analysis of slope channel architecture and fill. Marine and Petroleum Geology 41, 83–103.

Gardner, M.H., Borer, J.M., 2000. Submarine channel architecture along a slope to basin profile, Brushy Canyon Formation,West Texas. In: Bouma, A.H., Stone, C.G. (Eds.), Fine-Grained Turbidite Systems. Memoir 72-American Association of Petroleum Geologists and Special Publication 68-SEPM, pp. 195–214.

Gardner, M.H., Borer, J.M., Melick, J.J., Mavilla, N., Dechesne, M., Wagerle, R.N., 2003. Stratigraphic process-response model for submarine channels and related features from studies of Permian Brushy Canyon outcrops, West Texas. Marine and Petroleum Geology 20, 757–787.

Gingerich, P.D., 1969. Markov analysis of cyclic alluvial sediments. Journal of Sedimentary Petrology 39, 330–332.

Graham, S.A., Bachman, S.B., 1983. Structural controls on submarine fan geometry and internal architecture: Upper La Jolla Fan system, offshore southern California. AAPG Bulletin 67, 83–96.

Hansen, L.A.S, 2016. Architecture and sedimentology of submarine channel-related thin-bedded turbidites. Ph.D. Thesis. University of Aberdeen.

Hansen, L.A.S., Callow, R.H.T., Kane, I., Gamberi, F., Rovere, M., Cronin, B.T., Kneller, B.,

2015. Genesis and character of thin-bedded turbidites associated with submarine channels. Marine and Petroleum Geology 67, 852–879.

Hansen, L. Callow, R. Kane, I., Kneller, B., 2017. Differentiating submarine channel related thin-bedded turbidite facies: Outcrop examples from the Rosario Formation, Mexico. Sedimentary Geology 358, 19 – 34.

Harper C.W.Jr. 1984. Improved methods of facies sequence analysis. In: Walker R.G. (Ed.): Facies models. Geoscience Canada, Reprint Series 1, pp. 11 – 13.

Haughton, P.D.W., 2000. Evolving turbidite systems on a deforming basin floor, Tabernas, south-east Spain. Sedimentology 47, 497 – 518.

Haughton, P.D.W., Barker, S.P., McCaffrey, W.D., 2003. “Linked” debrites in sand-rich turbidite systems - origin and significance. Sedimentology 50, 459 – 482.

Haughton, P., Davis, C., McCaffrey, W., Barker, S., 2009. Hybrid sediment gravity flow deposits: classification, origin and significance. Marine and Petroleum Geology 26, 1900 – 1918.

Heard, T.G., Pickering, K.T., 2008. Trace fossils as diagnostic indicators of deep-marine environments, Middle Eocene Ainsa-Jaca basin, Spanish Pyrenees. Sedimentology 55, 809 – 844Hein, F.J., Walker, R.G., 1982. The Cambro-Ordovician Cap Enrage Formation, Quebec, Canada: conglomeratic deposits of a braided submarine channel with terraces. Sedimentology 29, 309 – 352.

Hein, F.J., Robb, G.A., Wolberg, R.A., Longstaffe, F.J., 1991. Facies descriptions and associations in ancient reworked (?transgressive) shelf sandstones: Cambrian and Cretaceous examples. Sedimentology 38, 405 – 431.

Hodgson, D.M., Di Celma, C.N., Brunt, R.L., Flint, S.S., 2011. Submarine slope degradation and aggradation and the stratigraphic evolution of channel-levee systems. Journal of the Geological Society of London 168, 625 – 628.

Hubbard, S.M., Romans, B.W., Graham, S. A., 2008. Deep-water foreland basin deposits of the Cerro Toro Formation, Magallanes basin, Chile: architectural elements of a sinuous basin axial channel belt. Sedimentology 55, 1333 – 1359.

Hubbard, S.M., Covault, J.A., Fildani, A., Romans, B.W., 2014. Sediment transfer and deposition in slope channels: deciphering the record of enigmatic deep-sea processes from outcrop. Geological Society of America Bulletin 126, 857 – 871.

Jackson, C.A.L., Barber, G.P., Martinsen, O.J., 2008. Submarine slope morphology as a control on the development of sand-rich turbidite depositional systems: 3D seismic analysis of the

Kyrre Fm (Upper Cretaceous), Måløy Slope, offshore Norway. Marine and Petroleum Geology 25, 663 – 680.

Janocko, M., Nemec, W., Henriksen, S., Warchoł, M., 2013. The diversity of deep-water sinuous channel belts and slope valley-fill complexes. Marine and Petroleum Geology 41, 7 – 34.

Jobe, Z.R., Bernhardt, A., Lowe, D.R., 2010. Facies and architectural asymmetry in a conglomerate-rich submarine channel fill, Cerro Toro Formation, Sierra Del Toro, Magallanes Basin, Chile. Journal of Sedimentary Research 80, 1085 – 1108.

Kane, I.A., Kneller, B.C., Dykstra, M., Kassem, A., McCaffrey, W.D., 2007. Anatomy of a submarine channel–levee: an example from Upper Cretaceous slope sediments, Rosario Formation, Baja California, Mexico. Marine and Petroleum Geology 24, 540 – 563.

Kane, I.A., Dykstra, M.L., Kneller, B.C., Tremblay, S., McCaffrey, W.D., 2009. Architecture of a coarse-grained channel–levée system: the Rosario Formation, Baja California, Mexico. Sedimentology 56, 2207 – 2234.

Kane, I.A., Hodgson, D., 2011. Submarine channel levees: criteria for recognition of levee subenvironments: exhumed examples from the Rosario Fm. (Baja, Mexico) and the Laingsburg Fm. (Karoo Basin). Marine and Petroleum Geology 28, 807 – 823.

Knaust, D., Warchol, M., Kane, I.A., 2014. Ichnodiversity and ichnoabundance: revealing depositional trends in a confined turbidite system.Sedimentology 61, 2218–2267.

Kneller, B., Buckee, C., 2000. The structure and fluid mechanics of turbidity currents: a review of some recent studies and their geological implications. Sedimentology 47, 62 – 94.

Kneller, B., 2003. The influence of flow parameters on turbidite slope channel architecture. Marine and Petroleum Geology 20, 901 – 910.

Kneller, B., Martinsen, O.J., McCaffrey, W. (Eds.), 2009. External Controls on Deep-water Depositional Systems. SEPM Special Publication 92, 402 pp.

Kolla, V., Bandyopadhyay, A., Gupta, P., Mukherjee, B., Ramana, D.V., 2012. Morphology and internal structure of a recent upper Bengal fan-valley complex. In: Prather, B.E., Deptuck, M.E., Mohrig, D., Van Hoorn, B., Wynn, R.B. (Eds.), Application of the Principles of Seismic Geomorphology to Continental Slope and Base of Slope Systems: Case Studies from Seafloor and Near-Seafloor Analogues. SEPM Special Publication 99, pp. 347 – 369.

Krumbein, W.C., Dacey, M.F., 1969. Markov chains and embedded chains in geology. Journal of the International Association for Mathematical Geology 1, 79 – 96.

Li, P., 2017. Architecture and sedimentology of slope channel fills: an outcrop- and subsurface-

based study. Ph.D., University of Aberdeen. 196 pp.

Lehrmann, D.J., Rankey, E.C., 1999. Do meter-scale cycles exist? A statistical evaluation from vertical (1-D) and lateral (2-D) patterns in shallow-marine carbonates-siliciclastics of the "Fall In" strata of the Capitan Reef, Seven Rivers Formation, Slaughter Canyon, New Mexico. SEPM Special Publication 65, 51–62.

Li, P., Kneller, B.C., Hansen, L., Kane, I.A., 2016. The classical turbidite outcrop at San Clemente, California revisited: an example of sandy submarine channels with asymmetric facies architecture. Sedimentary Geology 346, 1–16.

Lowe, D.R., 1982. Sediment gravity flows: II. Depositional models with special reference to the deposits of high-density turbidity currents. Journal of Sedimentary Petrology 52, 279–297.

Macauley, R.V., Hubbard, S.M., 2013. Slope channel sedimentary processes and stratigraphic stacking, Cretaceous Tres Pasos Formation slope system, Chilean Patagonia. Marine and Petroleum Geology 41, 146–162.

Martini, I.P., Sagri, M., Doveton, J.H., 1978. Lithologic transition and bed thickness periodicities in turbidite successions of the Antola Formation, Northern Appeanines, Italy. Sedimentology 25, 605–623.

Mayall, M., Stewart, I., 2000. The architecture of turbidite slope channels. In: Weimer, P., Slatt, R.M., Bouma, A.H., Lawrence, D.T. (Eds.), Deep-Water Reservoirs of the World. Gulf Coast Section SEPM 20th Annual Research Conference, pp. 578–586.

Mayall, M., Jones, E., Casey, M., 2006. Turbidite channel reservoirs-key elements in facies prediction and effective development. Marine and Petroleum Geology 23, 821–841.

McArthur, A., Kneller, B.C., Souza, P.A., Kuchle, J., 2016. Characterization of deep-marine channel-levee complex architecture with palynofacies: An outcrop example from the Rosario Formation, Baja California, Mexico. Marine and Petroleum Geology 73, 157–173.

McHargue, T., Pyrcz, M.J., Sullivan, M.D., Clark, J.D., Fildani, A., Romans, B.W., Covault, J.A., Levy, M., Posamentier, H.W., Drinkwater, N.J., 2011. Architecture of turbidite channel systems on the continental slope: patterns and predictions. Marine and Petroleum Geology 28, 728–743.

Miall, A., 1973. Markov chain analysis applied to an ancient alluvial plain succession. Sedimentology 20, 347–364.

Morris, W., Busby-Spera, C.J., 1990. A submarine-fan valley-levee complex in the Upper

Cretaceous Rosario Formation: Implication for turbidite facies models. GSA Bulletin 102, 900 – 914.

Morris, W.R., Busby, C.J., 1996. The effects of tectonism on the high-resolution sequence stratigraphic framework of non-marine to deep-marine deposits in the Peninsular Ranges Fore-arc basin complex. In: Abbott, P., Cooper, J.D. (Eds.), Pacific Section SEPM Guidebook, Los Angeles, pp. 73 – 88.

Morris, E.A., Hodgson, D.M., Flint, S., Brunt, R.L., Luthi, S.M. and Kolenberg, Y., 2016. Integrating outcrop and subsurface data to assess the temporal evolution of a submarine channel–levee system. AAPG Bulletin 100, 1663– 1691.

Mutti, E., 1985. Turbidite systems and their relation to depositional sequences. In: Zuffa, G.G. (Ed.), Provenance of Arenites. NATO-ASI series, Reidel, Dordrecht, Netherlands, pp. 65 – 93.

Nelson, C.H. and Maldonado, A. 1988, Factors controlling depositional patterns of Ebro turbidite systems, Mediterranean Sea: AAPG Bulletin 72, 698 – 716.

Paull, C.K., Caress, D.W., Ussler III, W., Lundstern, E., Meiner-Johnson, M., 2011. High-resolution bathymetry of the axial channels within Monterey and Soquel submarine canyons, offshore central California. Geosphere 7, 1077 – 1101.

Paull, C.K., Caress, D.W., Lundsten, E., Gwiazda, R., Anderson, K., McGann, M., Conrad, J., Edwards, B., Sumner, E.J., 2013. Anatomy of the La Jolla Submarine Canyon system; offshore southern California. Marine Geology 335, 16 – 34.

Peakall, J., McCaffrey, B., Kneller, B., 2000. A process model for the evolution, morphology, and architecture of sinuous submarine channels. Journal of Sedimentary Research 70, 434 – 448.

Pickering, K. T., Hodgson, D. M., Platzman, E., Clark, J. D., Stephens, C., 2001. A new type of bedform produced by backfilling processes in a submarine channel, late Miocene, Tabernas-Sorbas basin, SE Spain. Journal of Sedimentary Research 71, 692 – 704.

Piper, D.J.W., Hiscott, R.N., Normark, W.R., 1999. Outcrop-scale acoustic facies analysis and latest Quaternary development of Hueneme and Dume submarine fans, offshore California. Sedimentology 46, 47 – 78

Pirmez, C., Beauboeuf, R.T., Friedmann, S.J., Mohrig, D.C., 2000. Equilibrium profile and baselevel in submarine channels: examples from Late Pleistocene systems and implications for the architecture of deepwater reservoirs. In: Weimer, R.M. Slatt, J.

Coleman, N.C., Rosen, H. Nelson, A.H. Bouma, M.J. Styzen, D.T.L. (Eds.), Deep Water Reservoirs of the World. GCSSEPM Foundation 20th Annual Research Conference, Houston, pp. 782 – 805.

Porter, M.L., Sprague, A.R.G., Sullivan, M.D., Jennette, R.T., Beaubouef, R.T., Garfield, T.R., Rossen, D., Sickafoose, D.K., Jensen, G.N., Friedmann, S.J., Mohrig, D.C., 2006. Stratigraphic organization and predictability of mixed coarse- and fine- grained lithofacies successions in a Lower Miocene Deep-water Slope-channel System, Angola Block 15. In: Harris, P.M., Weber, L.J. (Eds.), Giant Hydrocarbon Reservoirs of the World: From Rocks to Reservoir Characterization and Modeling. AAPG Memoir 88, 281 – 306 pp.

Posamentier, H.W., Kolla, V., 2003. Seismic geomorphology and stratigraphy of depositional elements in deep-water settings: Journal of Sedimentary Research 73, 367 – 388.

Powers, D.W., Easterling, R.G., 1982. Improved methodology for using embedded Markov chains to describe cyclical sediments. Journal of Sedimentary Petrology 52, 913 – 923.

Pyles, D.R., Jennette, D.C., Tomasso, M., Beaubouef, R.T., Rossen, C., 2010. Concepts learned from a 3D outcrop of a sinuous slope channel complex: Beacon Channel Complex, Brushy Canyon Formation, West Texas, U.S.A. Journal of Sedimentary Research 80, 67 – 96.

Romans, B.W., Normark, W.R., McGann, M.M., Covault, J.A., Graham, S.A., 2009. Coarse-grained sediment delivery and distribution in the Holocene Santa Monica Basin, California: implications for evaluating source-to-sink flux at millennial time scales. GSA Bulletin 121, 1394 – 1408.

Samuel, A., Kneller, B., Raslan, S., Sharp, A., Parsons, C., 2003. Prolific deep marine slope channels of the Nile Delta, Egypt. AAPG Bulletin 87, 541 – 560.

Sprague, A.R., Sullivan, M.D., Campion, K.M., Jensen, G.N., Goulding, F.J., Garfield, T.R., Sickafoose, D.K., Rossen, C., Jennette, D.C., Beaubouef, R.T., Abreu, V., Ardill, J., Porter, M.L., Zelt, F.B., 2002. The physical stratigraphy of deep-water strata: a hierarchical approach to the analysis of genetically related stratigraphic elements for improved reservoir prediction. AAPG Annual Meeting Abstracts, Houston, pp. 10 – 13.

Sprague, A.R.G., Garfield, T.R., Goulding, F.J., Beaubouef, R.T., Sullivan, M.D., Rossen, C., Campion, K.M., Sickafoose, D.K., Abreu, D., Schellpeper, M.E., Jensen, G.N., Jennette, D.C., Pirmez, C., Dixon, B.T., Ying, D., Ardill, J., Mohrig, D.C., Porter, M.L., Farrell, M.E., Mellere, D., 2005. Integrated slope channel depositional models: the key to successful

prediction of reservoir presence and quality in offshore West Africa, CIPM, cuarto E-Exitep. Veracruz, Mexico, pp. 1 – 13.

Staňová, S., Soták, J., Hudec, N., 2009. Markov Chain analysis of turbiditic facies and flow dynamics (Magura Zone, Outer Western Carpathians, NW Slovakia). Geologica Carpathica 60, 295 – 305.

Sylvester, Z., Pirmez, C., Cantelli, A., 2011. A model of submarine channel-levee evolution based on channel trajectories: implications for stratigraphic architecture. Marine and Petroleum Geology 28, 716 – 727.

Sullivan, M., Jensen, G., Goulding, F., Jennette, D., Foreman, L., Stern, D., 2000. Architectural analysis of deep-water outcrops: implications for exploration and development of the Diana sub-basin, western Gulf of Mexico. In: Weimer, P., Slatt, R.M., Coleman, J., Rosen, N.C., Nelson, H., Bouma, A.H., Styzen, M.J., Lawrence, D.T. (Eds.), Deep-Water Reservoirs of the World. GCSSEPM Foundation 20th Annual Research Conference, pp. 1010 – 1031.

Sumner, E.J., Talling, P.J., Amy, L.A., Wynn, R.B., Stevenson, C., Frenz, M., 2012. Facies architecture of individual basin-plain turbidites: comparison to existing models and implications for flow processes. Sedimentology 59, 1850 – 1857.

Terlaky, V., Rocheleau, J., Arnott, R.W.C., 2016. Stratal composition and stratigraphic organization of stratal elements in an ancient deep-marine basin-floor succession, Neoproterozoic Windermere Supergroup, British Columbia, Canada. Sedimentology 63, 136 – 175.

Thompson, P., 2010. The spatial and temporal variation of stratigraphic elements within the San Fernando Channel System, Baja California, Mexico. Unpublished Ph.D. Thesis. University of Aberdeen.

Walker, R.G., 1975. Nested submarine-fan channels in the Capistrano Formation, San Clemente, California. Geological Society of America Bulletin 86, 915–924.

Walker, R.G., 1985. Mudstones and thin-bedded turbidites associated with the Upper Cretaceous Wheeler Gorge conglomerates, California: A possible channel-levee complex. Journal of Sedimentary Petrology 55, 279 – 290.

Wild, R.J., Hodgson, D.M., Flint, S.S., 2005. Architecture and stratigraphic evolution of multiple, vertically-stacked slope-channel complexes, Tanqua depocentre, Karoo Basin, South Africa. In: Hodgson, D.M., Flint, S.S. (Eds.), Submarine Slope Systems, Processes and Products. Geological Society of London Special Publication 244, pp. 89 – 112.

Wilkinson, B.H., Glen, K., Merrill, G.K., Kivett, S.J., 2004. Stratal order in Pennsylvanian cyclothems: Reply: GSA Bulletin 116, 1545–1550.

Winn, R.D., Dott, R.H., 1979. Deep-water fan-channel conglomerates of Late Cretaceous age, southern Chile. Sedimentology 26, 203–228.

Wonham, J.P., Jayr, S. Mougamba, R., Chuilon, P., 2000, 3D sedimentary evolution of a canyon fill (lower Miocene age) from the Mandorove Formation, offshore Gabon. Marine and Petroleum Geology 17, 175–197.

Wuellner, D.E., James, W.C., 1989. Braided and meandering submarine fan channel deposits, Tesnus Formation, Marathon Basin, West Texas. Sedimentary Geology 62, 27–45.

Wynn, R.B., Cronin, B.T., Peakall, J., 2007. Sinuous deep-water channels: genesis, geometry and architecture. Marine and Petroleum Geology 24, 341–387.